RSC Advances

PAPER

View Article Online
View Journal | View Issue

Cite this: *RSC Adv.*, 2025, **15**, 18123

Gold(I) and gold(III) complexes of triazolyl-functionalised NHCs†

Hawraa S. Al-Buthabhak, *[a] Karrar Al-Ameed, [ab] Yu Yu,[cd] Alexandre N. Sobolev,[e] Stephen A. Moggach, [e] Hani Al-Salami,[f] Vito Ferro [g] and Murray V. Baker *[e]

Received 15th April 2025
Accepted 7th May 2025

DOI: 10.1039/d5ra02655e

rsc.li/rsc-advances

Novel triazolyl-functionalised imidazolium salts and their corresponding Au^{I}/Au^{III} complexes were synthesised and characterised by spectroscopic techniques and X-ray diffraction studies. The reaction of (mono and bis carbene) Au^{I} complexes with thionyl chloride gave Au^{III} complexes. These Au^{III} complexes are reduced to Au^{I} complexes by DMSO dissolution, and react with silver nitrate to afford chelating complexes, where the triazolyl N atoms bind to gold. The triazolyl-functionalised Au^{I} complexes showed potency against ovarian cancer cells (OVCAR-8 cells, IC_{50} < 15 μM).

Introduction

N-Heterocyclic carbenes (NHCs) are well known as ligands having strong donor properties akin to those of phosphines. Generally, however, highly functionalised NHCs are more readily accessible than phosphines, since they can be conveniently generated from air-stable azolium salts[1,2] and an array of other stable precursor compounds.[3–6] The ready synthetic accessibility of functionalised NHCs has meant that properties of metal–NHC complexes, such as lipophilicity and steric bulk around the metal, can easily be tailored to a broad range of applications, including catalysis,[7–13] imaging,[14–20] and chemotherapy.[21–30] In cases where robust metal–NHC complexes are required, stability can be enhanced by incorporation of the NHC moiety into a multidentate or a pincer ligand.[31–33]

An interesting type of NHC results from combining an imidazolium salt and a triazole in the same compound by applying an azide–alkyne cycloaddition or "click" reaction.[34] One application of triazoles obtained by the click reaction is their use as ligands in metal complexes.[35] 1,2,3-Triazole ligands have been used previously for the generation of well-defined abnormal/mesoionic complexes of palladium, ruthenium, iridium, copper, silver, gold and platinum in which the triazolyl ligand binds to the metal centre as a carbene.[33,35–40] 1,2,3-Triazolyl ligands have also been used to form triazolyl–gold complexes in which the triazolyl unit binds to gold *via* C (as an abnormal carbene) or N, and these complexes have been tested for their catalytic activity.[33,39,41–43] The triazolyl–Au complexes or triazolyl–Au complexes having hemilabile ligands have proven to be efficient catalysts for enone formation from propargylic esters and alcohols,[42] for intermolecular hydroamination of amines with alkynes,[41] for formation of oxazolines by condensation of aldehydes and isocyanides,[39] and for synthesis of γ-substituted γ-butyrolactones.[40]

Combining triazolyl-type ligands with NHCs in the same ligand framework could lead to interesting properties and coordination modes of the resulting complexes.[38,44] For example, chelating triazolyl-functionalised NHC ligands (Tz-NHCs) have been used in combination with ruthenium in the transfer hydrogenation of ketones.[38] Similar ligand structures have been used in medicine,[45] metallopolymers,[44] and supramolecular chemistry.[46] Gold complexes derived from imidazolium salts that contain triazolyl units attached at the imidazolyl C4 or C5 positions have been reported.[45,47] Tubaro and coworkers have reported Au–NHC complexes of Tz-NHC ligands where the Tz units are pendant from the N of the NHC ring, but the Tz-NHC ligands did not chelate the Au centre.[48,49] In this work the synthesis of both neutral and cationic Au^{I} complexes of two new Tz-NHCs is reported. The Au^{I} complexes were then oxidised to give the corresponding Au^{III} complexes. The anticancer activity of some of these complexes was investigated in OVCAR-8 (ovarian cancer) cells. The new Tz-NHC ligands include a bromine atom to allow the possibility of using the

[a]*Department of Chemistry, Faculty of Science, University of Kufa, P. O. Box 21, Najaf 54001, Iraq. E-mail: hawraas.dawood@uokufa.edu.iq*

[b]*Department of Engineering, University of Warith Al-Anbiyaa, Karbala, Iraq*

[c]*Curtin Medical School, Curtin Health Innovation Research Institute, Curtin University, Perth, WA, 6102, Australia*

[d]*Division of Obstetrics & Gynaecology, The University of Western Australia Medical School, Perth, WA 6009, Australia*

[e]*School of Molecular Sciences M310, The University of Western Australia, 35 Stirling Highway, Perth, WA 6009, Australia. E-mail: murray.baker@uwa.edu.au*

[f]*Biotechnology and Drug Development Research Laboratory, Curtin Medical School & Curtin Health Innovation Research Institute, Curtin University, Perth, WA, 6102, Australia*

[g]*School of Chemistry and Molecular Biosciences, The University of Queensland, Brisbane, QLD, 4072, Australia*

† Electronic supplementary information (ESI) available. CCDC 2416356–2416359. For ESI and crystallographic data in CIF or other electronic format see DOI: https://doi.org/10.1039/d5ra02655e

NanoSIMS technique to track the fate of Au complexes in cells in future imaging studies.[50]

Results and discussion

Synthesis of triazolyl-functionalised imidazolium salts

The synthetic pathway to the triazolyl-functionalised imidazolium salts is shown in Scheme 1. It relies on applying the copper catalysed azide–alkyne cycloaddition reaction to appropriate azide and alkyne coupling partners. The known azide **2** was obtained in high yield (83%) from 2-bromobenzyl bromide **1** by treatment with sodium azide at room temperature in dimethylformamide.[51] Azide **2** was then reacted with 1-methyl-3-propargylimidazolium chloride **3** by adapting a literature procedure,[38] using catalytic amounts of a Cu/$CuSO_4$ mixture under heating at reflux. After workup, which included filtration through a column of silica gel, the triazolylimidazolium salt **5** was obtained as a brown oil in 45% yield. Using a similar procedure, reaction of azide **2** with 1,3-dipropargylimidazolium chloride **4** gave the new triazolylimidazolium salt **6** as a tan solid in 77% yield.

Synthesis of Au–NHC complexes having pendant triazolyl groups

Two neutral Au^I–NHC complexes **7** and **8** were then prepared by reacting imidazolium salts **5** and **6** with silver oxide according to a well-known literature procedure (Scheme 2).[52] The presumed intermediate Ag–NHC complexes derived from **5** and **6** are treated *in situ* with dimethylsulfide gold chloride [$(Me_2S)AuCl$] in one-pot reactions. Complex **7** was obtained as an off-white powder in relatively low yield (31%). Significant losses occurred due to the need for the material to be recrystallised twice, initially from acetonitrile/diethyl ether, and then from ethyl acetate at 0 °C, to achieve satisfactory purity. On the other hand, complex **8** was obtained as a white powder in 77–96% yield by filtration either through a plug of silica (4 : 1 DCM/MeCN) or Celite, followed by precipitation with DCM/hexanes.

The cationic bis-NHC Au^I complexes **9** and **10** were prepared by reaction of the salts **5** and **6** and with ~0.5 equivalents of $(Me_2S)AuCl$ in the presence of potassium carbonate[53] (8–10 equiv.) in acetonitrile (Scheme 2). Workup of **9** was straightforward and the compound was obtained as an off-white powder in 86% yield. Compound **10** was poorly soluble in acetonitrile, so during workup the acetonitrile was evaporated and the residue dissolved in ethanol. Filtration through Celite followed by evaporation of the solvent and washing with diethyl ether then gave **10** as a white powder in 72% yield.

In terms of solubility, it should be noted that both salts **5** and **6** are soluble in H_2O but differ in their solubility profile for less polar solvents, with salt **6** being soluble in DCM, while salt **5** is not. The neutral complexes **7** and **8** and the cationic complex **9** are all soluble in DCM but are insoluble in water. The cationic complex **10** is the only complex to show good solubility in water, but it is not soluble in DCM.

Oxidation of the triazolyl-functionalised Au^I–NHC complexes

Synthesis of Au^{III}–NHC complexes *via* oxidation of Au^I–NHC complexes with thionyl chloride. The reaction of Au^I–NHC complex **8** with thionyl chloride (220 equiv.) in DCM at reflux for ~44 h produced Au^{III} complex **12** in nearly quantitative yield (Scheme 3). Attempts to oxidise **8** using only a small excess (12 equiv.) of thionyl chloride at room temperature were not successful. In this experiment, the starting material **8** was the only compound detected by ^1H NMR spectroscopy in aliquots taken from the reaction mixture after 16 and 40 hours, respectively. Adding further thionyl chloride (~200 equiv.) to the

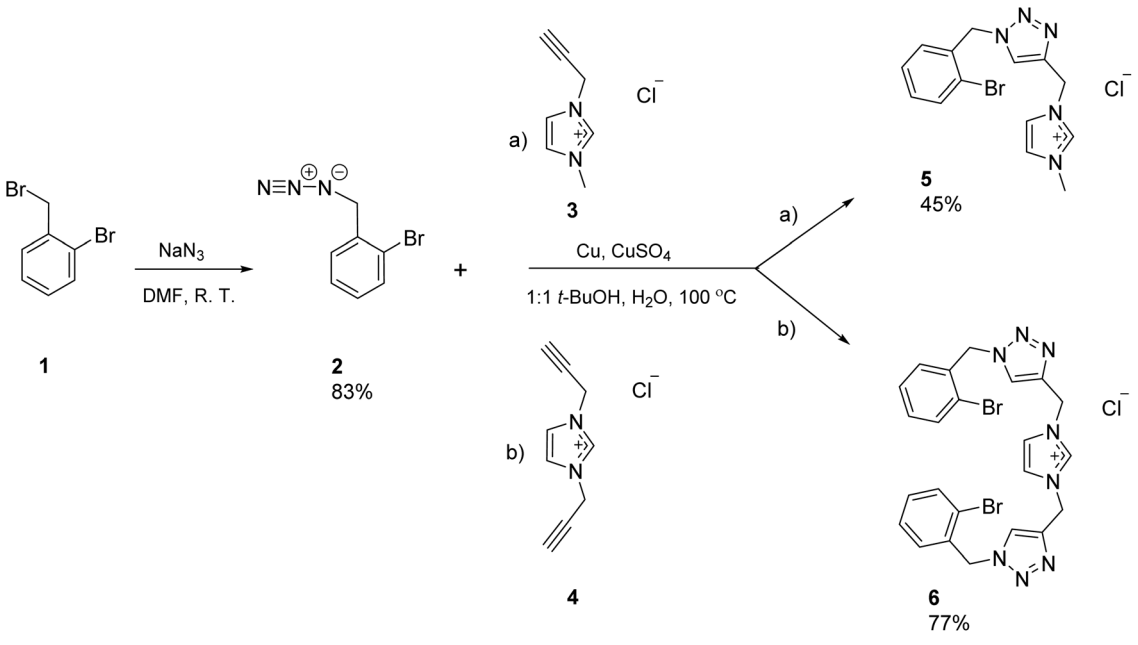

Scheme 1 Synthesis of triazolylimidazolium chloride salts **5** and **6**.

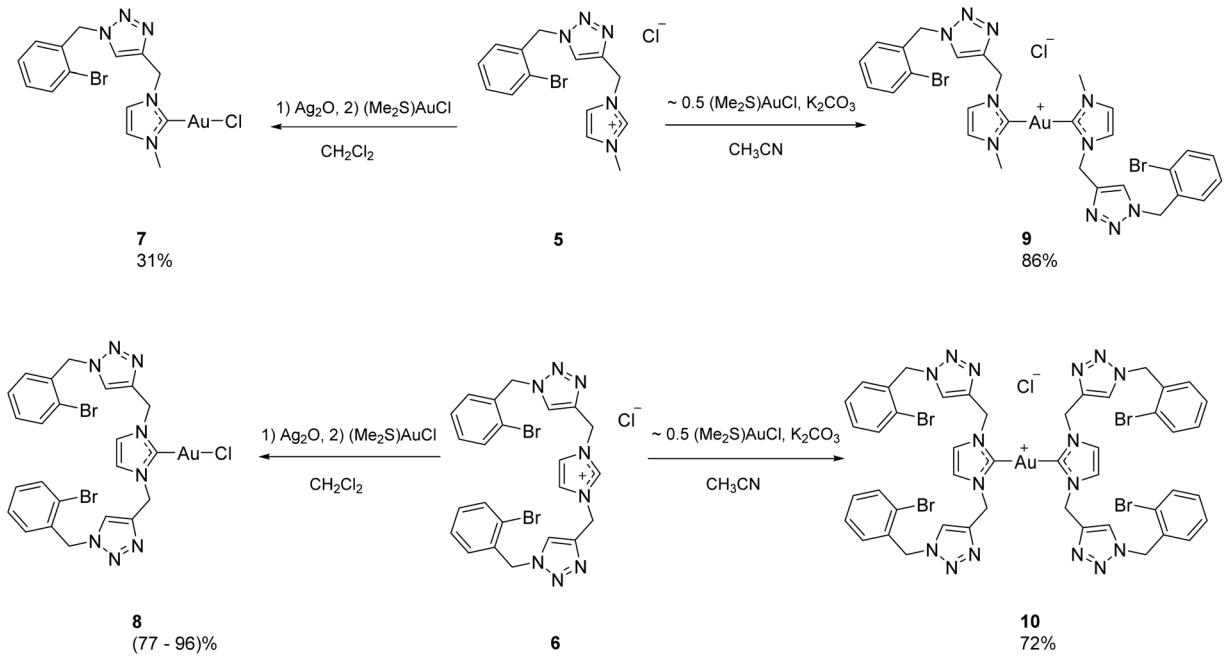

Scheme 2 Synthesis of the Au^{I}–NHC complexes having pendant triazolyl groups.

reaction mixture, and heating at reflux for a further 26 h, resulted in a mixture of the Au^{III} complex **12** and the Au^{I} complex **8** in a ratio of 4 : 1 respectively, and the reaction had gone to completion after heating at reflux for a further 22 h (total time at reflux ~48 h). Removal of volatiles under vacuum and washing of the residue with diethyl ether left the Au^{III} complex **12** as a yellow powder, in excellent yield (97%) and purity that is completely free from **8** (Fig. S5†). The choice of $SOCl_2$ oxidizing agent is vital, the ESI† describes complications encountered upon employment of $KAuCl_4$ and I_2.

While the NMR spectrum of trichloride **12** (Fig. S5†) in CD_2Cl_2 suggests a single species in solution, **12** converts to the monochloride **8** in DMSO-d_6. For example, the ^{1}H NMR spectrum of **12** in DMSO-d_6 showed **12** as the primary complex present immediately after preparation, but with trace **8** also detected (Fig. S7, top spectrum†). After 44 h, about a third of complex **12** had been reduced back to **8**, and after 25 days, the sample contained only **8** (Fig. S7, bottom spectrum†). The ESI† describes even greater apparent solution instability of related iodo analogues.

Curiously, **12** showed similar stability in acetone-d_6 and DMSO-d_6, even though DMSO is a more strongly coordinating solvent. A sample prepared by dissolving **12** in acetone-d_6 was monitored by ^{1}H NMR spectroscopy (Fig. S8†). After 4 days, the sample contained **8** and **12** in a ratio of ~1 : 1. In this experiment, a drop of water was added to the sample after 5 days, to see if water made the reversion of **12** to **8** occur more rapidly. The ^{1}H NMR spectrum recorded immediately after addition of water showed a similar ratio of **8** and **12** seen in the ^{1}H NMR spectrum recorded a day previously, indicating that addition of water did not immediately cause **12** to be reduced to **8**, but nevertheless after 13 days, no **12** remained in the sample.

In view of the encouraging results obtained using thionyl chloride for the oxidation of Au^{I}–NHC complex **8** to Au^{III} complex **12**, similar oxidations were explored for Au^{I} complexes of the form $[Au(NHC)_2]^+$, **9** and **10**. Complex **9** was oxidised to

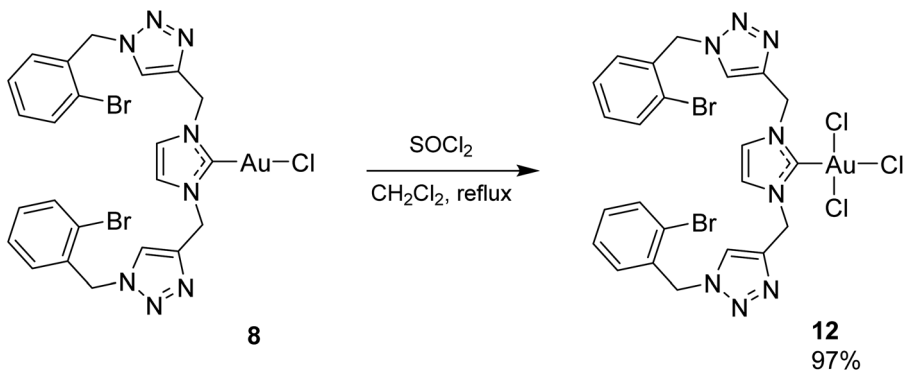

Scheme 3 Oxidation of Au^{I}–NHC complex **8** to Au^{III}–NHC complex **12** by $SOCl_2$.

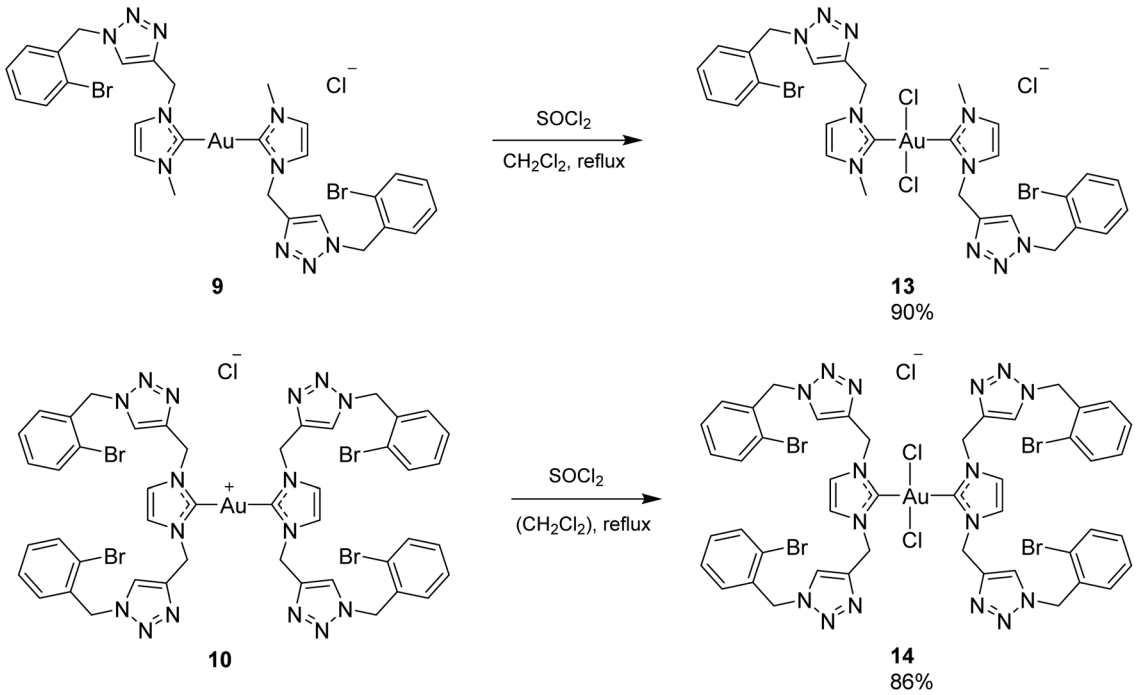

9 **13** 90%

10 **14** 86%

Scheme 4 Oxidation of bis Au^{I}–NHC complexes by $SOCl_2$.

Au^{III} complex **13** by treatment with excess thionyl chloride in DCM under reflux for 4 days. After workup complex **13** was obtained as a pale yellow powder in 90% yield (Scheme 4).

In the same way, oxidation of the bis Au^{I}–NHC **10** with excess thionyl chloride gave the Au^{III} complex **14** as a yellow powder in 86% yield (Scheme 4). In this case, however, the starting material **10** was poorly soluble in DCM. When **10** was stirred in DCM a cloudy suspension was obtained, but when $SOCl_2$ was added a clear solution formed. Interestingly, **10** is soluble in thionyl chloride, so the oxidation of **10** to **14** could be achieved simply by addition of neat reagent without any DCM, and the yield of **14** was >80% in both variations.

The pure compounds **13** and **14** are not soluble in DCM or acetone, and while **13** has only very limited solubility in acetonitrile, **14** is insoluble in this solvent. Fortunately, **13** and **14** were both soluble and sufficiently stable in DMSO-d_6 that they could be characterised by NMR spectroscopy in freshly-prepared DMSO-d_6 solutions. Nevertheless, the complexes slowly reverted to their Au^{I} precursors in DMSO-d_6, and for **14**, NMR spectra of even freshly prepared solutions showed signals due to traces of **10**. Elemental analyses of both **13** and **14** indicated that both complexes were pure, suggesting that the traces of **10** seen in NMR spectra of **14** were due to reduction of **14** by reaction with the solvent.

Comparing different pathways to access Au^{III} complexes. The work described above shows that oxidation of Au^{I}–NHC complexes by thionyl chloride affords isolable Au^{III} compounds. Employment of $SOCl_2$ was much more successful than our attempts with I_2 or $KAuCl_4$ as oxidants (see Section 1.1 of the ESI†). There is literature precedence for the importance of a chlorinating oxidiser in stabilising Au^{III} centres.[54] Furthermore, the approach to Au^{III}–NHC complexes *via* oxidation of Au^{I}–NHC complexes by thionyl chloride is superior to an approach by directly reacting $KAuCl_4$ with Ag–NHC complexes. This finding is consistent with a number of previous studies that showed that reaction of Au^{III} salts with sources of NHCs is invariably complicated by reduction to Au^{I} (ref. 55–57) (see ESI†).

Another important finding here is that the choice of solvent is significant because Au^{III} complexes **11–14** can be easily reduced, especially **11**, which is reduced immediately in DMSO-d_6. By avoiding DMSO-d_6 and acetone-d_6 and utilising less polar and non-coordinating solvents such as dichloromethane-d_2, reduction of Au^{III} to Au^{I} is minimised. This finding is consistent with reports by Hirtenlehner *et al.*[58] of the ease of reduction of Au^{III}–NHC complexes to Au^{I}–NHC complexes, although those studies were primarily focused on photo-reductions and there was no comment on DMSO as a potential reductant. The present study emphasizes the importance of solvent on stability of Au^{III}–NHC complexes, even though some Au^{III}–NHC complexes are stable DMSO-d_6.[58]

It is not surprising that **11–14** are easily reduced to their Au^{I} counterparts as previous studies have shown that Au^{III}–NHCs can be easily reduced to Au^{I}–NHCs by such reducing agents as phosphines, sulfides[59] or when chloropyridine is utilised as the solvent of the reaction.[55,56,60] In addition, it has been reported that when some Au^{III}–NHC complexes are utilised as pre-catalysts for hydration of alkynes, reduction to Au^{I}–NHC complexes occurred.[61]

Studies of Au–NHC complexes by NMR spectroscopy

^{1}H NMR spectroscopy was the primary tool used to monitor reactions and identify products of reactions explored in this

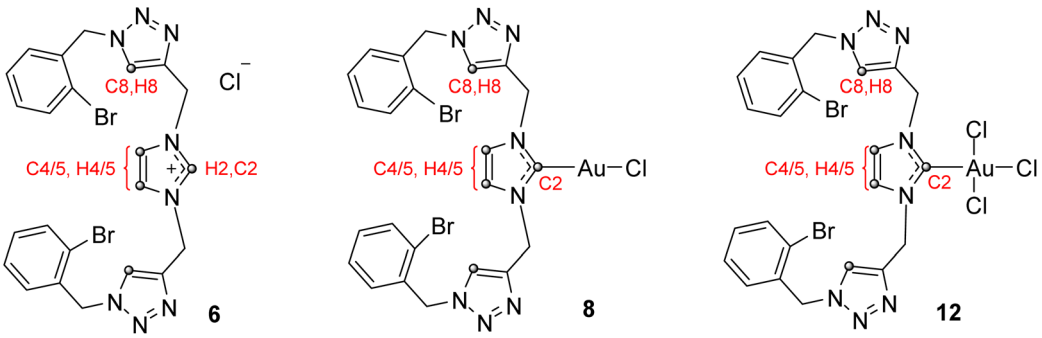

Scheme 5 Informative ^{1}H and ^{13}C environments for characterisation.

work. ^{1}H and ^{13}C NMR spectra of the new Tz-Im salts **5** and **6** and the corresponding Au^{I} and Au^{III} complexes are consistent with the structures determined by X-ray crystallography. ^{1}H and ^{13}C NMR chemical shifts seen for **5** and **6** and the corresponding Au^{I} and Au^{III} complexes are in the ranges seen for similar compounds reported in the literature.[6,22,30,56,58,62–64] The NMR signals associated with the imidazolyl and triazolyl moieties of the imidazolium salts and NHC complexes (*e.g.*, Scheme 5) are particularly informative. Changes in signals associated with imidazolyl and triazolyl moieties were used as indicators of coordination of these moieties to Au. Signals due to other protons and carbons showed little variation in splitting patterns or chemical shifts whether they arose from an imidazolium salt, an Au^{I} complex, or an Au^{III} complex.

Consider, for example, the ^{1}H NMR spectra for the Tz-Im salt **6** and the corresponding Au^{I} complex **8** and Au^{III} complex **12** shown in Fig. 1. The ^{1}H NMR spectrum of the salt **6** in DMSO-d_6 shows three downfield singlets, due to the imidazolium H2 proton (9.36 ppm), the triazole ring proton (8.27 ppm) and the H4/H5 protons (7.77 ppm). These signals are in the regions expected based on previous reports for similar compounds.[38] Signals for the protons of the aromatic ring are seen in the region 7.0–7.6 ppm and are well-resolved, and the protons of the two methylene groups occur as singlets at 5.7 ppm (C9 methylene, between the triazolyl and phenyl rings) and 5.5 ppm (C6 methylene, between triazolyl and imidazolyl rings). When **6** was treated with Ag_2O followed by $(Me_2S)AuCl$, formation of the corresponding Au^{I} complex **8** was indicated by the disappearance of the ^{1}H NMR signal at 9.36 ppm due to the imidazolyl

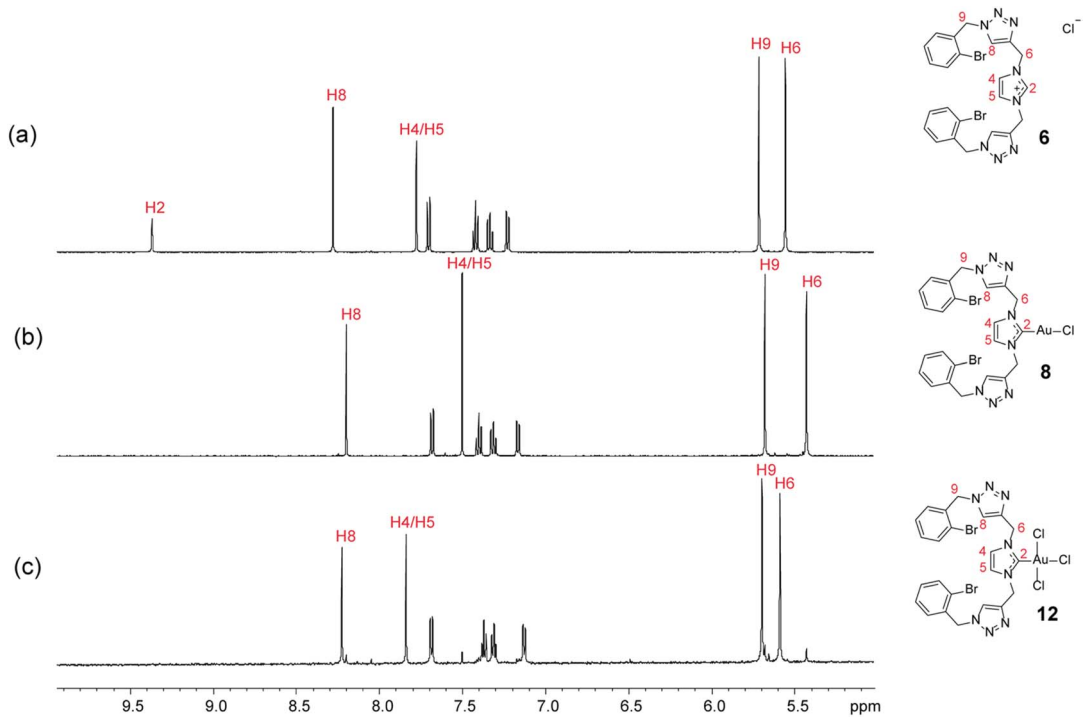

Fig. 1 ^{1}H NMR spectra (DMSO-d_6) of: (a) the imidazolium salt **6** showing the characteristic downfield signal for the H2 proton at 9.36 ppm; (b) the Au^{I}–NHC complex **8**; and (c) the Au^{III}–NHC complex **12**. Spectra (a) and (b) were recorded at 500 MHz, and spectrum (c) was recorded at 600 MHz.

proton (Fig. 1(b)). The other significant differences between the ^{1}H NMR spectra of **6** and **8** were the chemical shifts due to the H4/H5 protons (7.49 ppm, shifted upfield from 7.77 ppm for **6**) and C6 methylene protons (5.46 ppm, shifted upfield from 5.5 ppm for **6**). These upfield shifts can be attributed to the decrease in the Lewis acidity[65] of the substituent at the imidazolyl C2 position, H in **6** compared to Au^I in **8**. When the Lewis acidity of the substituent on C2 decreases, there is less withdrawal of the electron density from the imidazolyl ring, resulting in increased electronic shielding of the H4/H5 protons and the C6 methylene protons. The other protons in **8**, being more remote from C2 and the effects of the substituent on C2, have chemical shifts quite close to their counterparts in **6**.

In the ^{1}H NMR spectrum of **12** (Fig. 1(c)), the chemical shifts of the H4/H5 and C6 methylene protons are shifted significantly downfield of their counterparts in **8**, and slightly further downfield than their counterparts in **6**. These shifts for **12** can be attributed to the $Au^{III}Cl_3$ substituent at the imidazolyl C2 being a substantially stronger Lewis acid than the Au^ICl substituent in **8**, due to the electron withdrawing effects of Au^{III} and the three attached electronegative chlorine atoms. Again, the other protons in **12**, being more remote from C2 and the effects of the substituent on C2, show little difference in chemical shifts to their counterparts in **6** or **8**. Similar trends in ^{1}H NMR chemical shifts were seen for the key protons in the other Au complexes discussed herein, and are summarized in Table S2.†

In the ^{13}C NMR spectra of compounds **5** and **6** and the corresponding Au^I and Au^{III} complexes, for most carbons there is little variation in chemical shifts amongst the series imidazolium salt/Au^I–NHC complex/Au^{III}–NHC complex *etc.* For example, amongst all of compounds **5** and **6** and their corresponding Au^I and Au^{III} complexes, the ^{13}C chemical shifts of the triazolyl C8 carbons all fall within the range 122–126 ppm and the ^{13}C chemical shifts of the imidazolyl C4/C5 carbons all fall within the range 121–126 ppm (Table S3†). The C2 (carbene) carbons, however, show huge differences in chemical shifts within the series imidazolium salt/Au^I–NHC complex/Au^{III}–NHC complexes and interesting trends are evident (Table S3†). The chemical shifts of the carbene carbons fall into narrow but very distinct ranges depending on the class of compound: imidazolium salts ~ 136 ppm; (NHC)Au^ICl ~ 169 ppm; (NHC)$Au^{III}X_3$ 140–141 ppm; $Au^I(NHC)_2$ ~ 183 ppm; $Au^{III}(NHC)_2Cl_2$ 151–152 ppm. These ranges show that oxidation state of Au, as well as the ligands attached to Au, cause significant differences in the chemical shift of the carbene carbon. In all cases, the carbene chemical shift for Au^{III} complexes is about 30 ppm upfield of the carbene chemical shift for Au^I complexes, which has been attributed to the increased Lewis acidity of Au^{III} compared to Au^I causing increased delocalisation of electron density from the imidazolyl C4–C5 double bond to the carbene carbon *via* the imidazolyl aromatic system.[56]

Syn and *anti* isomerism of Au^{III} complex 13

Oxidation of the Au^I complex **9** by excess of thionyl chloride in DCM led to formation of the Au^{III} complex **13** (Scheme 4). The ^{1}H NMR spectrum of **13** (Fig. S6†) showed two distinct sets of signals, indicating the presence of two species in a ratio of 62 : 38, but elemental analysis was consistent with the elemental composition expected for **13** (with traces of occluded CH_2Cl_2). When the temperature was increased, various signals for the two species broadened and coalesced, resulting in an "averaged" spectrum at high temperature (Fig. S10†), indicating that the two species interconvert on the NMR timescale. The two species detected by NMR spectroscopy are therefore assigned as *syn* and *anti* conformations of **13** that differ by the orientation of the NHC moieties about the C–Au–C axis (Scheme 6).

The existence of two observable conformations of **13** presumably results from the square planar geometry of Au^{III} complex **13** and steric bulk provided by the chlorido ligands on Au, which can restrict the rotation of NHC ligands around the C–Au^{III}–C axis. Two conformations are not seen in the case of the Au^I complex **9** because, without the bulk provided by additional chlorido ligands on the Au centre, there is no substantial barrier to rotation of the NHC ligands about the C–Au^I–C axis. This sort of conformational isomerism has been reported previously for other square planar complexes of the form $M(NHC)_2X_2$.[1,58,66,67] Intuitively, the dominant conformation is expected to be *anti*-**13**, since the *syn* conformation would be destabilised by unfavourable steric interactions between the bromobenzyltriazolyl moieties. The ^{1}H–^{1}H ROESY NMR spectrum for a sample containing *anti*-**13** and *syn*-**13** showed a correlation between the signals due to the CH_3 and H6 protons of the major isomer, but not for the minor isomer. The observed correlation is consistent with the assignment of the major isomer as *anti*-**13**, since in this conformation the CH_3 protons in one NHC ligand will be close in space to the H6 protons of the other NHC ligand. In *syn*-**13**, the CH_3 protons in

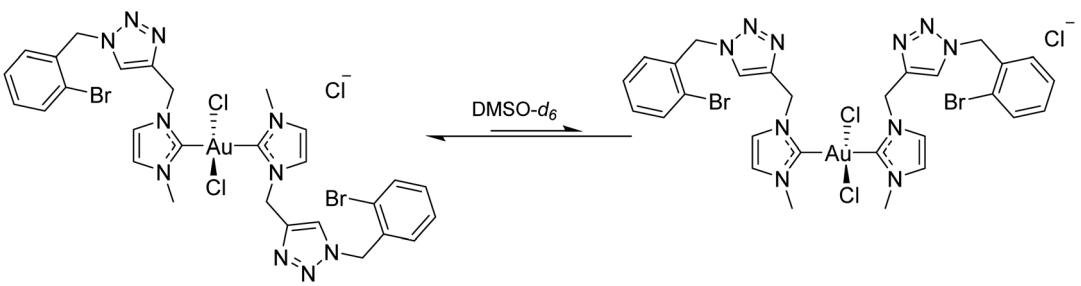

Scheme 6 *Syn* and *anti* conformers of Au^{III} complex **13**.

one NHC ligand are remote from both the H6 protons in the same NHC ligand and the H6 protons in the other NHC ligand.

The variable temperature NMR study of **13** in DMSO-d_6 (Fig. S10†) shows various signals broadening and coalescing as the temperature is raised. This behaviour is reversible, as expected for an NMR exchange process involving interconversion of conformations. Two sets of signals, for the CH_3 groups and for the imidazolyl H4 protons in the *syn* and *anti* conformations, are sufficiently well-separated that they can be integrated in the room temperature spectrum. Integration of these signals indicated that ratio of the populations of nuclei in the *anti* and *syn* conformations is 62 : 38 respectively. At room temperature, the chemical shift separation for the signals due to the CH_3 protons of the two conformations is 50.0 Hz, and coalescence of those signals occurs at ~338 K (Fig. S10†). Similarly, the chemical shift separation for the signals due to the imidazolyl H4 protons of the two conformations is 30.0 Hz, and coalescence of those signals occurs at ~328 K (Fig. S10†).

For an exchange between equally populated sites, the rate constant k at the coalescence temperature (the temperature at which signals of the exchanging nuclei are just merged together) can be estimated as $k = 2.22\Delta\nu$, where $\Delta\nu$ is the chemical shift separation (in Hz) of the nuclei in the absence of exchange.[68] In the case of the interconversion of *anti*-**13** and *syn*-**13**, the populations of exchanging nuclei are unequal (see ESI†).

The results in (Table S1†) appear to be reasonable. The rate constants increase with temperature as expected, and the relative size of the rate constants for the *anti* → *syn* and the *syn* → *anti* processes are consistent with the observed ratio of *anti*-**13** : *syn*-**13** in solution. In principle, it should be possible to calculate values for $\Delta S^{\ddagger}$ and $\Delta H^{\ddagger}$[69] from the results in (Table S1†), but the uncertainty in the coalescence temperature is probably too large for such calculations to be meaningful.

The results in (Table S1†) are in the range seen for the results of previous studies for the interconversion of *syn* and *anti* conformations of Au^{III}–NHC complexes. Hirtenlehner *et al.*[58] used quantum chemical calculations to estimate the barrier to rotation for interconversion of *syn* and *anti* conformations of a $[(NHC)_2Au^{III}Br_2]^+$ complex as ~60 kJ mol^{-1}, but noted that the result was not consistent with their ^{1}H NMR study (200 MHz, DMSO-d_6). In their NMR study, ^{1}H NMR signals separated by ~40 Hz at room temperature were not near coalescence even when the temperature was raised to 90 °C, indicating a high rotational barrier, expected to be significantly greater than 60 kJ mol^{-1}. Huynh and Wu[70] estimated the rotational barrier for *syn*/*anti* interconversion in a [*trans*-$(NHC)_2PdBr_2$] complex to be 74 kJ mol^{-1}, from ^{1}H NMR experiments in which the coalescence occurred at high temperature (380 K). None of these studies appear to have taken into account of the population difference between *anti* and *syn* conformations in their analyses.

Computational conformational analysis of **13** was also used to explore the experimental observation of two species in a ratio 62 : 38 in the NMR spectrum of **13** for *anti* : *syn* isomers, respectively. This suggests a significant preference for the *anti*-conformation under the studied conditions. Computational calculations support this finding, indicating that the *anti* isomer is more stable by 2.0 kcal mol^{-1} compared to the *syn* form (see Fig. 3). While this energy difference is not exceptionally large, it is sufficient to largely suppress the population of the *syn* isomer at equilibrium. The reported ΔE was used only to qualitatively support the observation that the *anti* isomer is energetically favored, rather than to quantitatively reproduce the NMR-derived *syn* : *anti* ratio. According to Boltzmann distribution principles, even differences as small as 1–2 kcal mol^{-1} can result in a dramatic shift in population at room temperature.[71] This has been demonstrated in several experimental and computational studies. For example, in a study on azomethine derivatives, the *anti* isomer was favoured by only ~1.8 kcal mol^{-1}.[72] Similarly, in a study on losartan isomers, the *anti* conformation was more stable and dominant in NMR spectra.[73] These findings underscore that even moderate energy differences can dictate the dominant species in solution. Therefore, while 2.0 kcal mol^{-1} might seem modest, it is more than sufficient to explain why the *anti* conformer is the dominant species form the ratio in the NMR spectrum of **13**.

Like the Au^{III} complexes **11** and **12**, the Au^{III} complex **13** was unstable in DMSO. For example, in DMSO-d_6 solution, ~50% of the Au^{III} complex **13** had been reduced to the corresponding Au^{I} complex **9** after 4 days, and little **13** remained after 25 days (Fig. S9†).

Halide abstraction reactions of Au^{III} complexes of Tz-NHC ligands: the quest for chelate Au^{III}–NHC complexes

Au^{III}–NHC complexes in which the Au centre is chelated by a functionalised NHC ligand are interesting for their potential use as catalysts.[74] Chelation should stabilise the Au^{III} centre, allowing such complexes to participate in reactions as catalysts without the Au^{III} centre reverting to Au^{I}. In order to chelate the Au^{III} centre in complexes such as **12** and **13** to the N atoms of triazolyl rings, experiments to abstract chloride from the Au^{III} centres were explored. The goal was to facilitate displacement of the two chloride ligands of **12** and **13** with intramolecular coordination of the pendant triazolyl groups to from the proposed chelate complexes **15** and **16** (Scheme S3†).

Reaction of the $(NHC)AuCl_3$ complex 12 with $AgNO_3$

When complex **12** was treated with $AgNO_3$ in DMSO-d_6 solution in an NMR tube, a white precipitate (presumably AgCl) formed immediately. A new Au^{III}–NHC complex was formed and was assigned the structure **15**, in which the metal centre is chelated by the NHC unit and the two triazolyl units in the organic ligand (Scheme 7). When only 2.2 equivalents of $AgNO_3$ were used, **15** was formed as a mixture with the Au^{I}–NHC complex **8** in a ratio of 19 : 1, respectively. The two complexes were separated during workup based on their solubilities (**15** was insoluble in CH_2Cl_2 so **8** was easily removed by a simple washing step with CH_2Cl_2) and pure **15** was obtained as a white powder in 56% yield. Interestingly, when 3.3 equivalents of $AgNO_3$ was used (again in DMSO-d_6 in an NMR tube), **15** was the only complex formed. It may be that with excess Ag^+, abstraction of chlorido ligands from **12** occurs rapidly, so that the Au^{III} centre is quickly stabilised by chelation by the triazolyl moieties, whereas when less

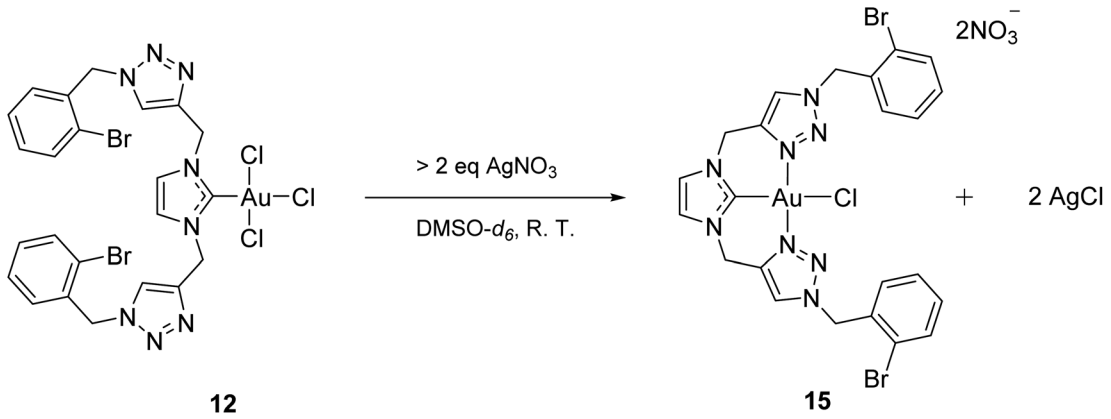

Scheme 7 Abstraction of chlorido ligands from **12** by Ag^+, to form **15**.

Ag^+ is used, the chelation occurs more slowly, allowing some time for **12** to be reduced to **8** as discussed above. Furthermore, the fact that the same product (**15**) was formed when **12** was treated with 2.2 or 3.3 equivalents of $AgNO_3$ indicates that Ag^+ is only able to abstract two chlorido ligands from **12**. Evidently **15** is resistant to abstraction of the final chlorido ligand from the Au centre. It may be that the result of such an abstraction, an Au^{III} centre chelated by an NHC and two triazolyl units, with the remaining coordination site either vacant or occupied by nitrate or DMSO, is unstable and so cannot be formed, or it may be that chelation provides kinetic stability to **15**.

It is interesting to compare these results with those of Hirtenlehner *et al.*,[58] who treated complexes of form $(NHC)AuBr_3$ and $[(NHC)_2AuBr_2]^+$ with Ag^+ in the presence of various anionic ligands L^-. In that study, the NHC ligand was 1,3-dibenzylimidazol-2-ylidene, which has no ability to chelate the Au^{III} centre. In every case, the starting Au^{III}–NHC complexes decomposed to form complicated mixtures containing Au^I species such as (NHC)AuL and $[(NHC)_2Au]^+$, in addition to Au(0) and imidazolium salts as the major products.

Unfortunately, attempts to obtain single crystals of **15** were not successful, so structure determination was based on the results of elemental analysis and NMR studies. Elemental analysis indicated an empirical formula $C_{23}H_{20}AuBr_2ClN_{10}O_6 \cdot (CH_2Cl_2)_{1.2}$, which is consistent with the structure proposed for **15** with some entrapped CH_2Cl_2 (used during workup). The ^1H NMR spectrum (Fig. 2) was also consistent with the structure **15** in terms of number of signals seen, their chemical shifts, and their relative integrals. Key signals are a 2H singlet at 9.03 ppm (assigned to the triazolyl protons), a 2H singlet at 7.99 ppm (assigned to the imidazolyl H4/H5 protons), and two 4H singlets at 6.1 and 5.8 ppm, assigned to the methylene groups adjacent to the bromophenyl and imidazolyl groups, respectively. Assignments of all ^1H NMR signals for **15** were carried out with the aid of ^1H–^{13}C HSQC and HMBC experiments. The number of signals (one signal for the H4/H5 protons, one for the two triazolyl protons, two signals for the four methylene groups, and one set of signals for the two bromophenyl groups) is consistent with a structure that has a plane of symmetry, as in the chelate complex **15** where both triazolyl groups are bound directly to the Au centre. The possibility of one or both triazolyl groups being bound as an abnormal carbene (C–Au bond) can be discounted by the presence of the 2H signal for the triazolyl protons.

Comparison of the ^1H NMR spectra of **12** and **15** (both recorded in DMSO-d_6) is informative. The most significant difference between the two spectra is the chemical shift of the signal for the triazolyl protons (H8 in Fig. 2), which is shifted from ~8 ppm in **12** to ~9 ppm for **15**, consistent with the triazolyl N donating electron density to Au centre in **15**, leaving less electron density in the ring to shield the triazolyl proton. Both methylene signals are also shifted downfield in the spectrum of **15**, again consistent with coordination of the triazolyl groups to Au, resulting in electrons being withdrawn from the triazolyl ring causing deshielding of the methylene groups relative to the situation in **12**.

In the ^{13}C NMR spectrum of **15**, the key signals are those for the Au-bound carbon and the triazolyl carbon. In DMSO-d_6 solution the imidazolyl C2 carbon appears at 138.0 ppm and the triazolyl carbons (C8) appear at 128.1 ppm. These chemical shifts are quite close to those of the corresponding signals for **12**, for which C2 occurs at 140.9 ppm and C8 occurs at 125.1 ppm, but the comparison is problematic because the instability of **12** in DMSO made it necessary to record the ^{13}C NMR spectrum in CD_2Cl_2. Assignments of all ^{13}C and ^1H NMR signals for **15** were aided by ^1H–^{13}C HSQC and HMBC experiments.

To explore the stability of complex **15**, an NMR sample of **15** prepared by adding 3.3 equivalents of $AgNO_3$ to **12** in DMSO-d_6 was monitored for change over the course of one week (Fig. S11†). ^1H NMR spectra showed new signals emerging that did not match the chemical shifts of Au^I complex **8**, although new signals associated with protons of the bromophenyl moiety did appear in the region where the corresponding signals for **8** occurred. These observations suggest that decomposition might involve dissociation of one (or both) triazolyl groups from the Au centre, but not simply *via* some reduction process to form the Au^I complex **8**. Excess Ag^+ was present in the sample and may have been involved in additional reactions with **15**. Nevertheless, **15** was quite stable in the solution, and much more stable than its non-chelate counterpart **12**. Integration of

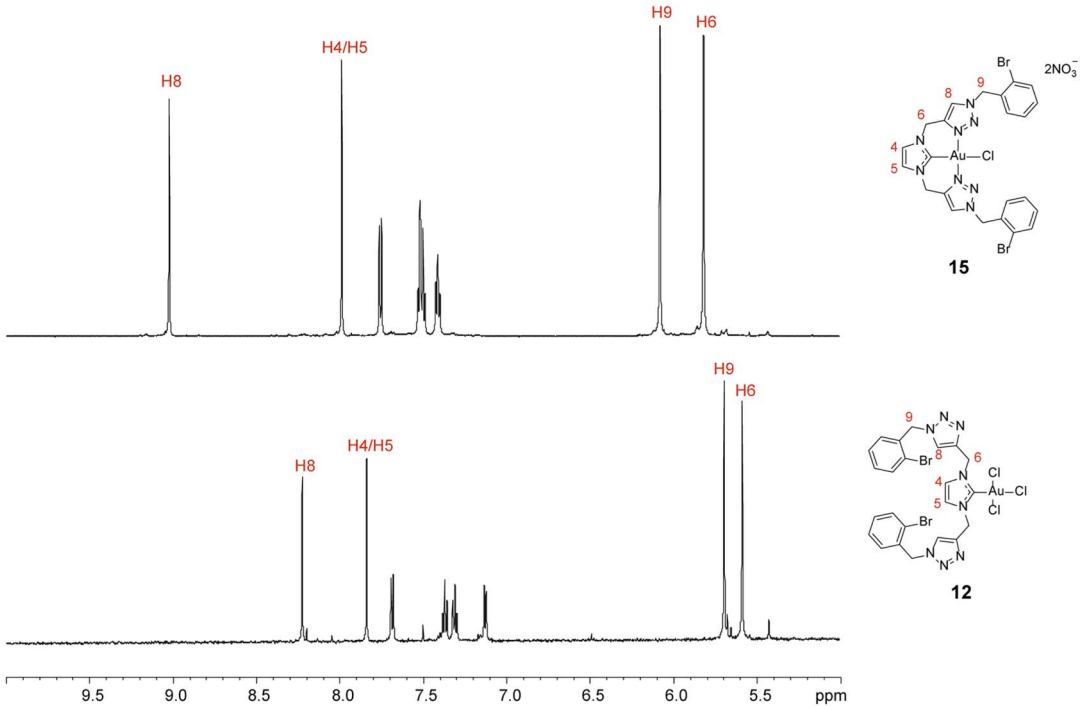

Fig. 2 ^{1}H NMR spectra (600 MHz, DMSO-d_6) of chelate complex **15** (top spectrum), and $Au^{III}Cl_3$ complex **12** (bottom spectrum).

the signal for the triazolyl proton (using the DMSO-d_6 solvent signal as an internal standard) showed that 86% of **15** remained after 22 h, and 55% remained after 7 days.

Furthermore, the origin of the pronounced stability observed for the closed form of the compound **15** was investigated, density functional theory (DFT) calculations were performed to compare two forms of compound **15**: tridentate N,N,C-Tz-NHC Au^{III} monochloride complex (closed form) *versus* hypothetical monodentate Tz-NHC Au^{III} monochloride complex (open form). In the proposed open structure, the compound adopts a linear coordination geometry, while the experimentally observed compound **15** exhibits a square planar coordination involving intramolecular interactions with nitrogen atoms from the adjacent five-membered rings. The calculations in Fig. 3 indicate that the closed form is energetically favored by 70.4 kcal mol^{-1} relative to the open form. This substantial energy difference not only underscores the thermodynamic preference for the closed conformation but also provides a compelling justification for why the open form has not been experimentally isolated. The strong stabilization arising from the Au–N chelation likely plays a pivotal role in stabilizing the closed geometry of compound **15**.

Reaction of the $[(NHC)_2AuCl_2]^+$ complex 13 with $AgNO_3$

In preliminary attempts to abstract chlorido ligands from **13** to form chelate complexes, KPF_6 was used as the chloride abstracting agent. However, several attempts to abstract chloride by treating **13** with KPF_6 in DMSO-d_6, at room temperature and at 50 °C, were unsuccessful. No evidence of chloride abstraction was seen and no precipitate was formed, indicating that the salt KCl (which would form if abstraction occurred) was not present in the mixtures. The only change seen in the samples was partial reduction of **13** to the Au^{I} complex **9**.

After these unsuccessful experiments to abstract the chlorido ligands by KPF_6, $AgNO_3$ was tested as the abstracting agent. When 3.4 equivalents of $AgNO_3$ was added to a solution of **13** in DMSO-d_6 in an NMR tube, a white precipitate (presumably AgCl) formed immediately. The ^{1}H NMR spectrum of the sample showed that none of **13** remained in the sample—both the *syn* and *anti* conformations of **13** had been consumed, and a complex mixture of products was formed (Fig. S12†).

Sadly, there were no ^{1}H NMR signals seen that could be confidently attributed to the desired product, the chelate complex **16** (Scheme S3†). Nevertheless, the ^{1}H NMR spectrum showed signals that are tentatively assigned to a chelate ligand in a species such as **17** (Scheme 8). One of the signals of interest here is a singlet at 9.11 ppm, which is tentatively assigned to the triazolyl proton H8 of a chelating triazolyl moiety, based on its strongly downfield chemical shift. The triazolyl H8 protons of the chelate complex **15** had a similar chemical shift. The other signals of interest are a group in the region 5.9–6.1 ppm. This group has the appearance of two doublets, but with small shoulders on either side of the group, suggesting that they may actually be two AB doublets. These signals are tentatively assigned to the C6 and C9 methylene protons, one AB pattern to each group. The integrals of the signal assigned to H8 and the C6 + C9 group are in the ratio 1 : 4 respectively, consistent with the tentative assignment.

The AB patterns arise because the two protons in each methylene group are rendered inequivalent by the asymmetry in **17** associated with the orientation of the non-chelating NHC

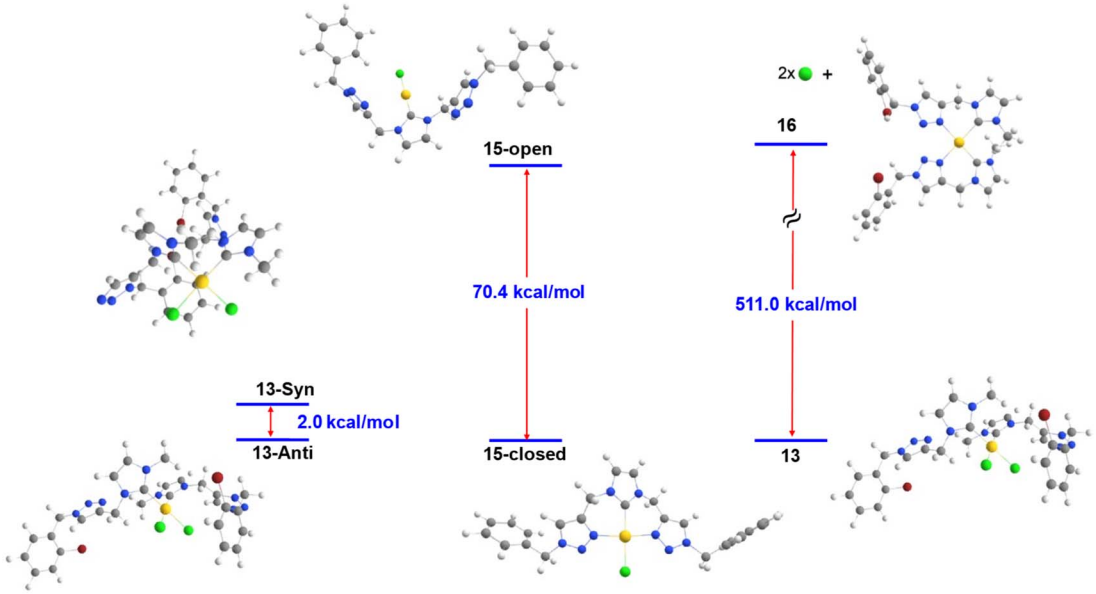

Fig. 3 The calculated relative stability of the complexes **13**, **15** and the attempted **16**: the atomic colors: gray; carbon, blue; nitrogen, green; chlorine, brown; bromide, yellow; gold, white; hydrogen.

ligand with respect to the C–Au–C axis. Interestingly, when the sample was heated (Fig. S13†), the two AB patterns collapsed to two singlets, which is consistent with interconversion of two isomeric conformations of **17** by rotation of the non-chelating NHC ligand about the C–Au–C axis (Scheme 8). Unfortunately, **17** was not stable at elevated temperatures, a significant proportion being decomposed when the sample was heated to 318 K and none remaining after the sample had been heated to 378 K (Fig. S13†), so the behaviour of **17** could not be explored in detail.

The species **17** is interesting as a potential precursor of **16** (Scheme S3†). Unfortunately, the species was formed as part of a complex mixture. The ^{1}H NMR spectrum of the mixture containing **17** and other products formed by treatment of **13** with $AgNO_3$ shows an envelope of signals at 5.5–5.9 ppm. These signals fall into the range seen for the methylene signals for

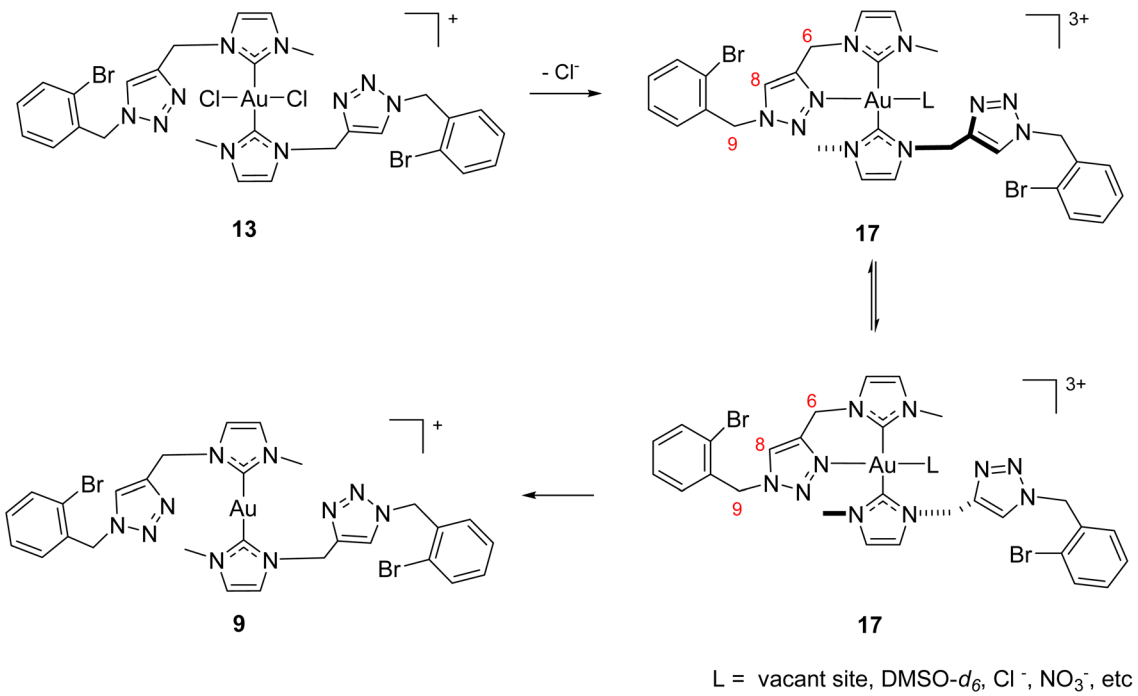

Scheme 8 Abstraction of Cl^- from Au^{III} complex **13** to form Au^{III} complex **17**, followed by reduction to form Au^{I} complex **9**.

anti- and *syn*-**13** (Fig. S6 and S10†), and are tentatively assigned to methylene signals associated with NHC ligands in which the triazolyl groups are not involved in chelation of the Au centre. Comparison of integrals for these signals and the signals assigned to the methylene groups of the chelating NHC ligand in **17** suggests that about 46% of **13** was converted to **17** and the remaining 54% was converted to other unidentified products. The mixture slowly underwent further change over time, to form the Au^{I} complex **9**. As noted above, formation of **9** was evident in the VT NMR study (Fig. S13†), but **9** was also formed in significant quantities in samples left at room temperature. Similarly, Hirtenlehner *et al.*[58] reported that attempts to abstract bromido ligands from $[(NHC)_2Au^{III}Br_2]^+Br$ (NHC = 1,3-dibenzylimidazolin-2-ylidene) by $AgNO_3$ resulted in partial or complete reduction to Au^{I}.

A comparative computational analysis of compound **13** with the attempted compound **16** is illustrated in Fig. 3. Although compound **16** has not been experimentally observed, the reaction energy calculations indicate a striking difference of over 500 kcal mol^{-1} in favour of compound **13**. This substantial stability suggests that compound **13** occupies a deep thermodynamic minimum, likely due to favourable electronic and structural factors that are absent in the structure of **16**.

X-ray diffraction studies

The structures of the imidazolium salt **6**·$2H_2O$, its (NHC)$Au^{I}Cl$ derivative **8**·$0.5Et_2O$, its (NHC)$Au^{III}ClI_2$ derivative **11** (see ESI†) and its (NHC)$Au^{III}Cl_3$ derivative **12** were characterised by X-ray crystallographic studies. Crystals suitable for X-ray analysis were grown by diffusion of vapours between pentane and a dichloromethane solution of the compound (for **6**, **11**, and **12**) or diethyl ether and a solution of the compound in acetone (for **8**).

In the solid-state structure of **6**·$2H_2O$, the cation was associated with one chloride counterion and two molecules of water (see Fig. S14,† which includes the atom numbering). The chloride ion shows weak interactions with an imidazolyl hydrogen (Cl(1)···H(3) 2.769 Å) and the triazolyl hydrogen (Cl(1)···H(25) 2.764 Å), smaller than the sum of the van der Waals radii as calculated by Bondi (2.95 Å)[75] and Alvarez (3.02 Å).[76] One water is involved in hydrogen bonding with an imidazolyl hydrogen (O(2)···H(4) 2.159 Å) and the other water is involved in hydrogen bonding with the triazolyl hydrogen (O(1)···H(55) 2.512 Å), both O···H distances being smaller than sum of the van der Waals radii as calculated by Bondi and Alvarez (2.72 and 2.70 Å respectively).[75,76] Interestingly, there appear to be no hydrogen bonding interactions involving the imidazolium N–CH–N hydrogen. The cation is in a trans-extended zig-zag conformation, with the three methylene carbons approximately coplanar, and the five rings being oriented approximately perpendicular to that plane (Fig. S15†). The cations are stacked into columns, perhaps stabilised by π-stacking interactions; the inter-centroid distance between opposing rings in adjacent cations is 4.467 Å (Fig. 4). Such arrangements can indicate weak parallel π–π interactions.[77]

The structure of **8**·$0.5Et_2O$ contains two independent molecules of **8**, one with disorder associated with one of its phenyl rings (Fig. 5). The Au–C distances are (Au(1)–C(11) 2.04(2), Au(2)–C(21) 2.03(2) Å), and Au–Cl distances are (Au(1)–Cl(1) 2.295(5), Au(2)–Cl(2) 2.294(5) Å). Coordination about Au is approximately linear (C(11)–Au(1)–Cl(1) 179.0(6)°, C(21)–Au(2)–Cl(2) 178.8(7)°). These distances and angles are in the ranges typically seen for (NHC)$Au^{I}Cl$ complexes.[64,78–80] The *N*-substituents on the NHC moiety are oriented *anti* to one another, with their N–C bonds in planes approximately orthogonal to the imidazolyl plane (Fig. 6).

In the structures of both **11** and **12** there are two independent molecules and the coordination modes for Au in the (NHC)$Au^{III}X_3$ seen in the structures of **11** and **12** are similar (see ESI, Fig. S16–S18†). The Au–$C_{carbene}$ and Au–X bond distances (see figure captions and Table S4†) are in the ranges seen in related compounds.[56,58,81–84] In **12**, the chlorido ligands *trans* to the NHC group has a longer Au–Cl bond (Au–Cl_{trans} 2.3078, 2.3215 Å) than for the chlorido ligands *cis* to the NHC group (Au–Cl_{cis} 2.2851, 2.2828, 2.2835, 2.2806 Å),[83] as expected due to the strong *trans* effect of the NHC ligand. In **12**, the Au is in a square planar coordination motif, with angles $C_{carbene}$–Au–Cl_{trans} ~ 176° and $C_{carbene}$–Au–Cl_{cis} in the range 87–89°. The Cl_{cis}–Au–Cl_{cis} angles are in the range 175.7–176.9°, with the chloride atoms pointing towards the carbene carbon. It has been suggested that this

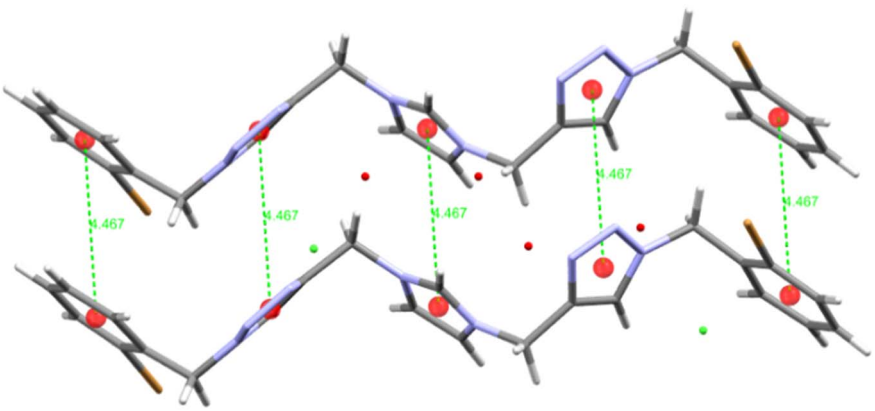

Fig. 4 Two adjacent cations in **6**·$2H_2O$, showing the inter-centroid spacings (4.467 Å) between opposing rings.

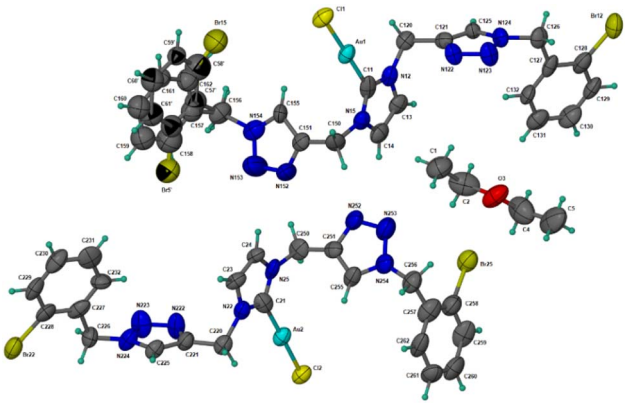

Fig. 5 Crystal structure of the **8**·0.5 Et_2O (50% probability level for the thermal displacement of ellipsoids). Selected bond distances (Å) and angles (°). Molecule 1: Au(1)–C(11), 2.04(2); Au(1)–Cl(1), 2.295(5); C(11)–Au(1)–Cl(1), 179.0(6); molecule 2: Au(2)–C(21), 2.03(2); Au(2)–Cl(2), 2.294(5); C(21)–Au(2)–Cl(2), 178.8(7).

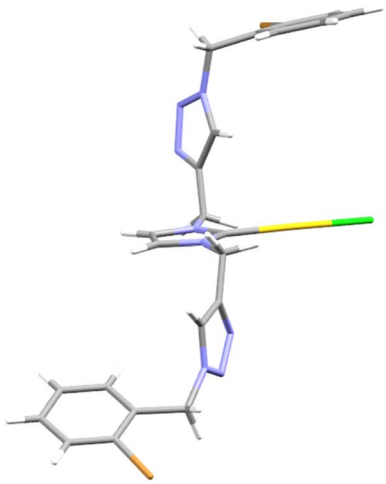

Fig. 6 One of the (NHC)AuCl molecules in **8**·0.5Et_2O, viewed close to the NHC plane, showing the pendant triazolyl groups with their triazolyl planes approximately orthogonal to the imidazolyl plane.

arrangement may be a consequence of an interaction between a chloride lone pair and the empty p-orbital on the carbene carbon.[81,85] Consistent with this suggestion, structures show $C_{carbene}\cdots Cl$ contacts ($C\cdots Cl_{cis}$ = 2.975–3.003 Å) that are substantially less than the sum of the van der Waals radii as calculated by Bondi (C···Cl 3.45 Å)[75] and Alvarez (C···Cl 3.59 Å).[76] The suggestion should be treated with some scepticism though, since the contacts between the Cl atom *trans* to the carbene C and the adjacent Cl atoms ($Cl_{trans}\cdots Cl_{cis}$ = 3.279–3.318 Å) are also less than the sum of the van der Waals radii as calculated by Bondi (Cl···Cl 3.50 Å)[75] and Alvarez (Cl···Cl 3.64 Å).[76]

In **12**, the triazolyl pendants are mutually *anti* about the imidazolin-2-ylidene moiety, creating a groove within which the Cl_{cis}–Au–Cl_{cis} moiety is located. The plane of the imidazolin-2-ylidene ring is inclined at an angle to the $CAuCl_3$ plane (θ in Fig. 7). The angle of inclination for the (NHC)$AuCl_3$ complex **12** (~69°).

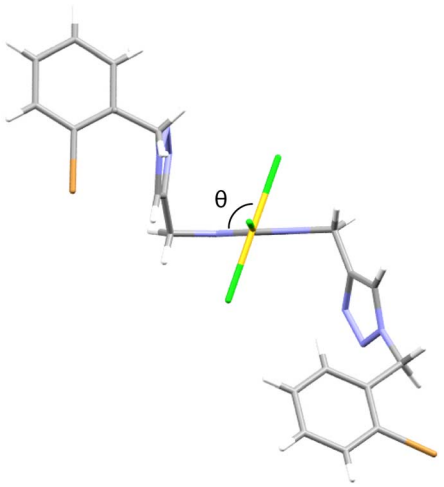

Fig. 7 View of the structure of the cation in **12** along the Cl_{trans}Au–$C_{carbene}$ axis. The plane defined by the imidazolyl ring in each case is horizontal and perpendicular to the page with the Cl_{trans} ligand in front of the page. The coordination plane for Au (defined by the Au centre and the Cl_{trans}, $C_{carbene}$) is also perpendicular to the page and inclined at an angle θ with respect to the plane of the imidazolyl ring. In **12**, θ = 68.68° (molecule 1) and 68.87° (molecule 2).

Activity of triazolyl-functionalised Au–NHC complexes against OVCAR-8 cells

Gold-based compounds, especially Au–NHC complexes, are receiving much attention due to their promising anti-cancer activity against a wide variety of cancer cell lines.[26,86,87] The dominant proposed mechanism for the activity of Au–NHCs is that Au inhibits the activity of mitochondrial thioredoxin reductase (TrxR) by binding to the soft Se and S atoms in the cysteine and selenocysteine residues at the active site.[24,26] TrxR is an important enzyme that regulates the cellular redox system and inhibition of TrxR can lead to a build-up of reactive oxygen species, which sets off a cascade of processes that leads to apoptosis (controlled cell death).[26,87,88] In this study, Au–NHC complexes were tested against OVCAR-8 ovarian cancer cells, a cisplatin-resistant cell line. Previous genetic profiling on OVCAR-8 suggested that it resembles high-grade serous ovarian carcinoma in patients (PMID 23839242), which is the most common histological subtype of ovarian cancer. A few classes of Au complexes, including auranofin and $[Au(dppe)_2]ClO_4$,[89] and imidazole-based complexes[90] have been tested in OVCAR-8 cells previously.

The activity of the triazolyl functionalised Au–NHC complexes **7**–**9** against OVCAR-8 cells is summarised in Table 1 and Fig. 8. The Au^{III} complexes **12** and **14** were not tested due to their instability in DMSO. The chelate Au^{III} complex **15** was not tested as it was only synthesised in small amounts, insufficient for biological testing.

The triazolyl functionalised Au–NHCs were active against the OVCAR-8 cells but showed higher IC_{50} values than the (NHC)

Table 1 IC_{50} values for triazolyl-functionalised Au–NHC complexes against OVCAR-8 cells[a]

Compound	IC_{50} (μM) ± SEM[c]	n
7	7.9 ± 1.3	4
8	13.2 ± 1.7	4
9	6.5 ± 0.1	3
6[b]	>100	3

[a] OVCAR-8 cells were exposed to test compounds during incubation for 72 h and activity of the compounds on cell viability was evaluated using an MTT assay. Data are shown as mean ± SEM of at least 3 independent experiments (n) each of which used 2 to 4 replicates per concentration for the relevant test compound. [b] Imidazolium salt **6** used as a negative control. [c] IC_{50} refers to the concentration of the drug that is required to inhibit the growth of the cancerous cell by 50%.

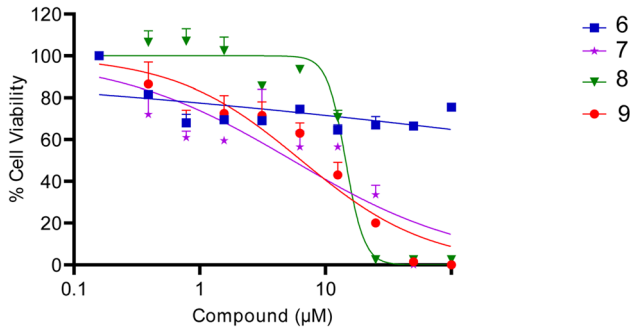

Fig. 8 The inhibition activity of the triazolyl-functionalised Au–NHC complexes against OVCAR-8 cells, measured by MTT assay after 72 h of treatment. The imidazolium salt 96 was used as negative control. Data are shown as mean ± SEM of at least 3 independent experiments, each of which used 2 to 4 replicates per concentration for the relevant test compounds.

Au(SCOR) complexes and $[(Pr_2Im)_2Au]Br$. From the IC_{50} values, the cationic bis-NHC complex **9** and the least hindered neutral (NHC)AuCl complex **7** are the most potent inhibitors, the more hindered neutral (NHC)AuCl complex being somewhat less active. Several factors likely contribute to activity in this series—the cationic nature of **9** (which would help it to target mitochondria), the hydrophilicity of the triazolyl groups, and different steric bulk around Au. The hydrophilic characteristic of the triazole moiety may decrease inhibitory activity, as Au compounds with greater hydrophobicity are typically more active than comparable hydrophilic ones.[24] In **8**, the steric bulk of the two bromophenylmethyltriazolyl groups may shield the Au centre from its biological targets, leading to decreased inhibitory activity of **8** compared to **7**; this shielding effect has been suggested previously.[23,91] Further work and a larger library of compounds are needed to provide further insights into the relative activities within the triazolyl-functionalised Au–NHC complexes.

Conclusions

The CuAAC click reaction of two propargyl-functionalised imidazolium salts with 2-bromobenzyl azide proceeded smoothly to form the corresponding triazolyl-functionalised imidazolium salts. The triazolyl-functionalised imidazolium salts were in turn converted into stable Au^I complexes of form (NHC)AuCl (*e.g.*, **8**) or $[(NHC)_2Au]Cl$ (*e.g.*, **10**). The triazole-functionalised (NHC)AuCl complexes could be oxidised by thionyl chloride to yield Au^{III} complex $(NHC)AuCl_3$. The complex was relatively stable in CD_2Cl_2 solution, but when dissolved in DMSO-d_6 the $(NHC)AuCl_3$ complex was reduced to the corresponding (NHC)Au^ICl complex, further studies of Au^{III}–NHC complexes focussed on chlorides rather than iodides.

Oxidation of $[(NHC)_2Au]Cl$ complexes with thionyl chloride gave the corresponding $[(NHC)_2Au^{III}Cl_2]Cl$ complexes, for example **13**, which was obtained as a mixture of *syn* and *anti* isomers. The $[(NHC)_2Au^{III}Cl_2]Cl$ complexes could be characterised by NMR spectroscopy in fresh DMSO-d_6 solutions, but were slowly reduced to $[(NHC)_2Au^I]Cl$, and poor solubility issues prevented their study in other solvents. The stability of Au^{III}–NHC complexes was improved by chelation. Treatment of the $(NHC)Au^{III}Cl_3$ complex **12** with $AgNO_3$ in DMSO-d_6 resulted in abstraction of the chloride ligands and formation of the chelated complex **15**, which showed good stability in DMSO-d_6.

The chelate compound **15** is a novel compound and it would be worthwhile to confirm the structure by X-ray diffraction. Further work could also be devoted to achieving the synthesis of the chelate complex **16**, which so far remains elusive. Efforts to react the Au^{III}–NHC complex **13** with $AgNO_3$ to form the doubly-chelate complex **16** have so far only led to a product tentatively assigned as **17**. Longer reaction times, more forcing reaction conditions, or the use of other chloride abstraction agents may permit **16** to be obtained.

Experimental section

General procedures

NMR spectra were recorded using Bruker AV500 III HD (500.13 MHz for ^1H, 125.77 MHz for ^{13}C, 202.45 MHz for ^{31}P), Bruker AV600 III HD (600.13 MHz for ^1H, 150.90 MHz for ^{13}C), or Bruker AV NEO (400.15 MHz for ^1H) spectrometers at ambient temperature, unless otherwise indicated. ^1H and ^{13}C NMR chemical shifts were referenced to the residual signal of the solvent (DMSO-d_6: ^1H 2.50 ppm; ^{13}C 39.52 ppm; CD_2Cl_2: ^1H 5.32 ppm; ^{13}C 53.8 ppm; acetone-d_6: ^1H 2.05 ppm; ^{13}C 29.84 ppm). Assignments of signals were confirmed with the aid of ^1H–^{13}C HSQC (heteronuclear single quantum coherence) and ^1H–^{13}C HMBC (heteronuclear multiple bond correlation) spectra when necessary. Microanalyses were performed by Microanalytical Service, School of Chemistry & Molecular Biosciences, The University of Queensland, Australia. High resolution mass spectra were measured using Agilent LCMS 6510 Q-TOF and Waters LCT Premier XE spectrometers, using the APCI or ESI methods, with 9 : 1 CH_3CN : H_2O as solvent. All the reactions were performed under a nitrogen atmosphere, in oven dried glassware. $(Me_2S)AuCl$ was prepared *via* the literature method.[92] Gold complexes were wrapped in aluminium foil to exclude light. Solvents were of analytical or reagent grade and used without further purification.

Computational methodology

All structures were fully optimized using Density Functional Theory (DFT) with the unrestricted hybrid B3LYP functional[93,94] and the all-electron def2-TZVP basis set,[95] as implemented in the Gaussian 16 software package.[96] Grimme's D3 dispersion correction with Becke–Johnson damping (D3-BJ)[97] was applied to account for long-range dispersion interactions. Geometry optimizations were followed by analytical frequency calculations to confirm that the stationary points correspond to true minima on the potential energy surface, as indicated by the absence of imaginary frequencies in the Hessian matrix.

Single X-ray crystal diffraction

Crystallographic data were measured at 100(2) K on an Oxford Diffraction Gemini or an Oxford Diffraction Xcalibur X-ray diffractometer using Mo Kα or Cu Kα radiation. Following analytical absorption corrections and solution by direct methods, the structures were refined against F^2 with full-matrix least-squares using the SHELX program suite.[98] Unless stated differently below, all hydrogen atoms were added at calculated positions and refined by use of riding models.

Anti-cancer activity

Cell culture reagents. Rosewell Park Memorial Institute (RPMI-1640) medium (with L-glutamine and sodium bicarbonate), fetal bovine serum (FBS), and penicillin–streptomycin were obtained from Sigma-Aldrich. Cell culture medium consists of RPMI-1640 medium (with L-glutamine and sodium bicarbonate) supplemented with 10% v/v FBS and 1% v/v penicillin–streptomycin. Cells were dissociated during passaging using trypsin solution 0.05% in Hank's balanced salt solution (HBSS), and ethylenediaminetetraacetic acid (EDTA), without calcium or magnesium (Hyclone GE Healthcare Life Sciences). MTT (3-(4,5-dimethylthiazol-2-yl)-2,5-diphenyltetrazolium bromide) was obtained from Thermo Fisher. Phosphate buffered saline (PBS) was obtained from Astral Scientific. Stock solutions (10 mM) of test compounds were prepared in DMSO (cell culture grade), obtained from Bio-Strategy. DMSO (to dissolve the MTT after incubation step in the MTT assay) was obtained from Sigma-Aldrich.

Cell culture. Human ovarian cancer cells (OVCAR-8, from ATCC) were cultured in 75 cm^2 tissue culture flasks in cell culture medium (10 mL) at 37 °C under air (5% humidity, 5% CO_2). After being incubated for 2 days, the cells had reached ~80% confluency and were then passaged as follows. The medium was poured off, and the cells were detached by incubation and agitation with trypsin (3 mL) for 3–5 min at 37 °C. To neutralise the trypsin solution, cell culture medium (3 mL) was added, and the cell suspensions were transferred to Falcon tubes and centrifuged for 5 min at 1500 rpm. The supernatant was drawn off by pipette, and the cell pellet was resuspended in culture medium (10 mL). The cells were re-plated into three tissue culture flasks (2 mL cell suspension and 8 mL culture medium per flask) and incubated for two days. The cell culture medium was replaced after 1 day if the cells had shown substantial proliferation and confluency.

Cell viability assays. Stock solutions of Au–NHC compounds (10 mM) were prepared in DMSO and were stored at −20 °C until required. These stock solutions were serially diluted in cell culture medium. For cell viability assays, OVCAR-8 cells that had reached 80% confluency in the tissue culture flasks were used. For cell seeding, the cells were dissociated as described above, the cell number was counted using a hemocytometer, and the cells were suspended in culture medium at a final concentration of 2000 cells/100 μL. Cell viability was determined using the MTT assay following the previously published protocol.[99] Briefly, OVCAR-8 cells were seeded in polystyrene 96-well plates (Costar; 2000 cells in 100 μL culture medium per well) and incubated for 24 h. Aliquots of solutions of Au–NHC compounds in cell culture medium (100 μL) were added to the wells so that the final concentrations of Au–NHC complex in wells was 0.39, 0.78, 1.56, 3.125, 6.25, 12.5, 25, 50, or 100 μM. The cells with the Au–NHCs were then incubated for 72 h. The medium was then carefully and completely removed by multichannel pipette and replaced by fresh cell culture medium (90 μL per well) and MTT solution (5 mg per mL MTT dissolved in PBS, 10 μL), and the plates were agitated to ensure homogeneity of solutions. The plates were incubated at 37 °C for 2 h, then the solution was removed by multichannel pipette and replaced by DMSO (200 μL per well) to solubilise the formazan purple colour from the live cells. The absorbance at 570 nm (A_{570}) was measured using a plate reader (Ensight Multimode Plate Reader, PerkinElmer). Relative cell viability (%) was determined by comparison of A_{570} for wells that had contained cells treated with Au–NHC complexes with A_{570} for wells that contained cells in culture medium alone. GraphPad Prism 8 software was used to determine IC_{50} values from cell viability data and to plot graphs of cell viability as a function of concentration of the Au–NHC complexes. Imidazolium salts (precursors of NHC ligands) were used as negative controls for the cytotoxicity of the compounds to OVCAR-8 cells.

Synthesis

Triazolyl-functionalised imidazolium salt (5). 2-Bromobenzyl azide (0.27 g, 1.27 mmol), $CuSO_4$ (27.0 mg, 0.169 mmol) and copper powder (4.7 mg, 0.075 mmol) were added to a solution of 1-methyl-3-propynylimidazolium chloride (200 mg, 1.27 mmol) in 1 : 1 H_2O/*tert*-butanol (5 mL each). The mixture was heated at reflux for 4 h, then cooled to room temperature and the solvents were evaporated to dryness. The residue was dissolved in 1 : 3 EtOH/MeOH (200 mL) and filtered through a plug of silica. The filtrate was evaporated to dryness and to the oily residue was added EtOH. The resulting precipitate was filtered off and the green filtrate was evaporated to give a yellow/brown oil (210 mg, 45%) which was dried under a flow of N_2. ^{1}H NMR (500 MHz, DMSO-d_6): δ 9.24 (br s, 1H, H2), 8.29 (s, 1H, H8), 7.76 (1H, apparent t, splitting 1.7 Hz, H4), 7.71–7.69 (m, 2H, H5 and H14), 7.42 (1H, apparent td, "triplet" splitting 7.5 Hz, $^4J_{H,H}$ = 1.2 Hz, H12), 7.33 (1H, apparent td, "triplet" splitting 7.7 Hz, $^4J_{H,H}$ = 1.8 Hz, H13), 7.24 (1H, dd, $^3J_{H,H}$ = 7.5 Hz, $^4J_{H,H}$ = 1.7 Hz, H11),

5.71 (s, 2H, H9), 5.55 (s, 2H, H6), 3.80 (s, 3H, C$\underline{H_3}$). ^{13}C NMR (125.7 MHz, DMSO-d_6): δ 140.6 (C7), 136.7 (C2), 134.5 (C10), 133.0 (C14), 130.7 (C11), 130.6 (C13), 128.3 (C12); 125.0 (C8), 123.8 (C5), 123.0 (C15), 122.4 (C4), 53.3 (C9), 43.5 (C6), 35.8 ($\underline{C}H_3$). Microanalysis: found: C, 39.74; H, 4.82; N, 16.02%. $C_{14}H_{15}BrClN_5$ $(H_2O)_{3.2}$ requires C, 39.44; H, 5.06; N, 16.43. HRMS (ESI^+): calcd for $C_{14}H_{15}BrN_5$ [M − Cl^+], *m*/*z* 332.0511. Found, *m*/*z* 332.0507.

Triazolyl-functionalised imidazolium salt (6). 2-Bromobenzyl azide (0.318 g, 1.50 mmol) was added to a solution of 1,3-dipropynylimidazolium chloride (135 mg. 0.75 mmol) in 1 : 1 H_2O/*tert*-butanol (4 mL each), followed by addition of $CuSO_4$ (16.0 mg, 0.10 mmol) and copper powder (2.70 mg, 0.044 mmol). The mixture was heated at reflux for 4 h, then cooled to room temperature and the solvent evaporated under vacuum. The residue was dissolved in DCM (40 mL) and filtered; the filtrate then passed through plug of silica eluting with 4 : 1 DCM/MeOH. The solvents were evaporated and the sticky brown residue that was obtained was washed with diethyl ether (3 × 30 mL) and precipitated from DCM/hexane with cooling (ice bath) to leave a tan powder (350 mg, 77%). ^{1}H NMR (500 MHz, DMSO-d_6): δ 9.36 (1H, br t, $^4J_{H,H}$ = 1.6 Hz, H2), 8.27 (s, 2H, H8), 7.77 (2H, d, $^4J_{H,H}$ = 1.6 Hz, H4/H5), 7.70 (2H, dd, $^3J_{H,H}$ = 7.9 Hz, $^4J_{H,H}$ = 1.3 Hz, H14), 7.41 (2H, apparent td, "triplet" splitting 7.5 Hz, $^4J_{H,H}$ = 1.3 Hz, H12), 7.33 (2H, apparent td, "triplet" splitting 7.7 Hz, $^4J_{H,H}$ = 1.7 Hz, H13), 7.22 (2H, dd, $^3J_{H,H}$ = 7.5 Hz, $^4J_{H,H}$ = 1.8 Hz, H11), 5.71 (s, 2H, H9), 5.55 (s, 2H, H6). ^{13}C NMR (125.7 MHz, DMSO-d_6): δ 140.4 (C7), 136.3 (C2), 134.5 (C10), 132.9 (C14), 130.7 (C11), 130.6 (C13), 128.3 (C12); 125.1 (C8), 123.0 (C15), 122.8 (C4/C5), 53.1 (C9), 43.6 (C6). Microanalysis: found: C, 42.61; H, 3.85; N, 17.07% $C_{21}H_{23}Br_2ClN_8 \cdot (H_2O)_{2.7}$ requires C, 42.28; H, 4.07; N, 17.15%. HRMS (ESI^+): calcd for $C_{23}H_{21}Br_2ClN_8$ [M − Cl^+], *m*/*z* 567.0256. Found, *m*/*z* 567.0277.

Crystals suitable for X-ray diffraction studies were grown by diffusion of vapours between diethyl ether and a solution of the compound in acetonitrile.

The triazolyl-functionalised (NHC)AuCl complex 7. A mixture of Ag_2O (80.0 mg, 0.34 mmol) and the triazolyl-functionalised imidazolium salt **5** (160 mg, 0.43 mmol) in DCM (20 mL) was stirred at room temperature in the absence of light for two days. (Me_2S)AuCl (100 mg, 0.34 mmol) was added and the mixture was stirred overnight then filtered through a plug of silica. The filtrate was evaporated to dryness. The residue was triturated with diethyl ether (3 × 10 mL), recrystallised from acetonitrile/diethyl ether, then recrystallised again from EtOAc at 0 °C and dried under vacuum to afford the product as an off white powder (60 mg, 31%). ^{1}H NMR (500 MHz, DMSO-d_6): δ 8.18 (s, 1H, H8), 7.68 (1H, dd, $^3J_{H,H}$ = 7.8, $^4J_{H,H}$ = 1.2 Hz, H14), 7.48 (1H, d, $^3J_{H,H}$ = 1.8 Hz, H5), 7.43 (1H, d, $^3J_{H,H}$ = 1.8 Hz, H4), 7.40 (1H, apparent td, "triplet" splitting 7.5 Hz, $^4J_{H,H}$ = 1.2 Hz, H12), 7.31 (1H, apparent td, "triplet" spitting 7.8 Hz, $^4J_{H,H}$ = 1.7 Hz, H13), 7.16 (1H, dd, $^3J_{H,H}$ = 7.5 Hz, $^4J_{H,H}$ = 1.7 Hz, H11), 5.67 (s, 2H, H9), 5.42 (s, 2H, H6), 3.74 (s, 3H, C$\underline{H_3}$). ^{13}C NMR (125.7 MHz, DMSO-d_6): δ 169.0 (C2), 142.4 (C7), 134.7 (C10), 132.8 (C14), 130.4 (C11), 130.4 (C13), 128.3 (C12), 124.5 (C8), 123.0 (C4), 122.8 (C15), 121.6 (C5), 52.9 (C9), 45.4 (C6), 37.7 ($\underline{C}H_3$). Microanalysis: found: C, 30.32; H, 2.72; N, 11.89% $C_{14}H_{14}AuBrClN_5$ $(CH_3CH_2OCOCH_3)_{0.2}$ requires C, 30.53; H, 2.70; N, 12.03%.

The triazolyl-functionalised [$(NHC)_2$Au]Cl complex 9. K_2CO_3 (316 mg, 2.28 mmol) and the triazolyl-functionalised imidazolium salt **5** (84.4 mg, 0.228 mmol) in acetonitrile (20 mL) was stirred at room temperature for 15 min, then (Me_2S)AuCl (29.5 mg, 0.10 mmol) was added. The mixture was stirred 3 days, and examination of an aliquot by ^{1}H NMR spectroscopy showed that the reaction was complete. The mixture was filtered through Celite and the filtrate was evaporated to dryness. The residue was washed with diethyl ether, then crystallised from acetonitrile/diethyl ether to afford an off-white powder (77.5 mg, 86%). ^{1}H NMR (500 MHz, DMSO-d_6): δ 8.22 (s, 2H, H8), 7.65 (2H, dd, $^3J_{H,H}$ = 7.8, $^4J_{H,H}$ = 1.2 Hz, H14), 7.60 (2H, d, $^3J_{H,H}$ = 1.8 Hz, H5), 7.49 (2H, d, $^3J_{H,H}$ = 1.8 Hz, H4), 7.34–7.27 (m, 4H, H12 and H13), 7.15 (2H, dd, $^3J_{H,H}$ = 7.5 Hz, $^4J_{H,H}$ = 1.8 Hz, H11), 5.64 (s, 4H, H9), 5.51 (s, 4H, H6), 3.82 (s, 6H, C$\underline{H_3}$). ^{13}C NMR (125.70 MHz, DMSO-d_6): δ 183.1 (C2), 142.8 (C7), 134.5 (C10), 132.9 (C14), 130.5 (C11), 130.4 (C13), 128.2 (C12), 124.3 (C8), 123.4 (C4), 122.9 (C15), 122.2 (C5), 53.0 (C9), 45.1 (C6), 37.5 ($\underline{C}H_3$). Microanalysis: found: C, 35.48; H, 3.32; N, 14.66% $C_{28}H_{28}AuBr_2ClN_{10} \cdot (H_2O)_3$ requires C, 35.37; H, 3.60; N, 14.73%. HRMS (ESI^+): calcd for $C_{28}H_{28}Br_2N_{10}$ Au [M − Cl^+], *m*/*z* 589.0531. Found, *m*/*z* 589.0594.

The triazolyl-functionalised [$(NHC)_2Au^{III}Cl_2$]Cl complex 13. Thionyl chloride (1.5 mL, 20.7 mmol) was added to a solution of the triazolyl-functionalised [$(NHC)_2$Au]Cl complex **9** (44.0 mg, 0.049 mmol) in DCM (15 mL), and the mixture heated at reflux for 4 days under N_2. The solvent was removed under vacuum and the residue was triturated with diethyl ether (3 × 5 mL) to leave the product as a pale yellow powder (42.5 mg, 90%). ^{1}H NMR (600 MHz, DMSO-d_6) two isomers: δ 8.22 (s, 2H, H8, *anti*), 8.25 (s, 1.37H, H8 *syn*), 7.86 (s, 2H, H4 *anti*), 7.80 (s, 1.35H, H4 *syn*), 7.71–7.68 (br m, 7H, H5 and H14, *anti* and *syn*), 7.35–7.29 (br m, 7H, H12 and H13, *anti* and *syn*), 7.14–7.09 (br m, 4H, H11 *anti* and *syn*), 5.80 (s, 2.8H, H6, *syn*), 5.70 (s, 4H, H9, *anti*), 5.67 (s, 2.8H, H9, *syn*), 5.64 (s, 4H, H6, *anti*), 4.07 (s, 6H. C$\underline{H_3}$, *anti*), 3.97 (s, 4H, C$\underline{H_3}$). ^{13}C NMR (150.90 MHz, DMSO-d_6) Two isomers: δ 151.84 (C2, *syn*), 151.76 (C2, *anti*), 141.71 (C7, *anti*), 141.5 (C7, *syn*), 134.5 (C10), 132.9 (C14), 130.5 (C13), 130.4 (C11), 128.1 (C12), 125.4 (C5, *syn*), 125.1 (C5, *anti*), 125.0 (C8, *syn*), 124.8 (C8, *anti*), 124.5 (C4, *anti*), 124.1 (C4, *syn*); 122.8 (C15), 53.1 (C9, *anti*), 44.5 (C6, *anti*), 44.3 (C6, *syn*), 37.5 ($\underline{C}H_3$, *anti*), 37.3 ($\underline{C}H_3$, *syn*).

Microanalysis: found: C, 33.88; H, 2.90; N, 13.78% $C_{28}H_{28}AuBr_2C_{13}N_{10}$. $(CH_2Cl_2)_{0.5}$ requires C, 33.89; H, 2.89; N, 13.87%.

The triazolyl-functionalised (NHC)AuCl complex 8. A mixture of Ag_2O (28.0 mg, 0.12 mmol) and the bis(triazolyl) imidazolium salt **6** (100 mg, 0.165 mmol) in DCM (10 mL) was stirred at room temperature in the absence of light for 33 h. (Me_2S)AuCl (40.0 mg, 0.136 mmol) was added and the mixture was stirred overnight. The mixture was eluted through a plug of silica using 1 : 4 MeCN/DCM (500 mL). The filtrate was evaporated, the product precipitated by dissolving it in ~2 mL DCM and excess of hexanes. The product was collected and dried under vacuum to afford a white powder (105 mg, 96%). ^{1}H NMR

(500 MHz, DMSO-d_6): δ 8.19 (s, 2H, H8), 7.68 (2H, dd, $^3J_{H,H}$ = 7.8, $^4J_{H,H}$ = 1.2 Hz, H14), 7.49 (s, 4H, H4/H5), 7.39 (2H, apparent td, "triplet" splitting 7.5 Hz, $^4J_{H,H}$ = 1.2 Hz, H12), 7.30 (2H, apparent td, "triplet" splitting $^3J_{H,H}$ = 7.8 Hz, $^4J_{H,H}$ = 1.7 Hz, H13), 7.16 (2H, dd, $^3J_{H,H}$ = 7.5 Hz, $^4J_{H,H}$ = 1.7 Hz, H11), 5.67 (s, 4H, H9), 5.42 (s, 4H, H6). ^{13}C NMR (125.7 MHz, DMSO-d_6): δ 169.1 (C2), 142.2 (C7), 134.7 (C10), 132.8 (C14), 128.2 (C11), 130.4 (C13), 128.4 (C12), 124.5 (C8), 122.8 (C15), 121.9 (C4/C5), 53.0 (C9), 45.6 (C6). Microanalysis: found: C, 34.42, H, 2.32, N, 13.60% $C_{23}H_{20}AuBr_2ClN_8$ requires C, 34.50, H, 2.52, N, 13.99%. Crystals suitable for X-ray diffraction studies were grown by diffusion of vapours between pentane and a solution of the complex in dichloromethane.

Also, the work up can be by filtration through Celite using dichloromethane as a solvent to afford a white powder 85%.

The triazolyl-functionalised [(NHC)$_2$Au]Cl (10). A mixture of K_2CO_3 (106 mg, 0.76 mmol) and the bis(triazolyl)-functionalised imidazolium salt **6** (52.6 mg. 0.087 mmol) in acetonitrile (20 mL) was stirred at room temperature for 15 min. (Me$_2$S)AuCl (11.0 mg, 0.037 mmol) was added, and the mixture was stirred for two days. The solvent was removed under vacuum, the residue was dissolved in EtOH, and the mixture was filtered through Celite using EtOH. Removal of solvent and trituration of the residue with diethyl ether afforded the product as an off white powder (37 mg, 72%). ^{1}H NMR (500 MHz, DMSO-d_6): δ 8.24 (s, 4H, H8), 7.63 (4H, dd, $^3J_{H,H}$ = 7.6, $^4J_{H,H}$ = 1.4 Hz, H14), 7.60 (s, 4H, H4/H5), 7.29–7.28 (m, 8H, H12 and H13), 7.11 (4H, dd, $^3J_{H,H}$ = 7.5, $^4J_{H,H}$ = 2.1, H11), 5.61 (s, 8H, H9), 5.54 (s, 8H, H6). ^{13}C NMR (125.7 MHz, DMSO-d_6): δ 182.8 (C2), 142.5 (C7), 134.5 (C10), 132.9 (C14), 130.5 (C11), 130.4 (C13), 128.1 (C12), 124.5 (C8), 122.9 (C15), 122.5 (C4/C5), 53.0 (C9), 45.2. Microanalysis: found: C, 37.48; H, 2.58; N, 14.72% $C_{46}H_{40}$ $AuBr_4ClN_{16}\cdot(H_2O)_{0.5}$ $(CH_2Cl_2)_2$ requires C, 37.25; H, 2.93; N, 14.48%. HRMS (ESI$^+$): calcd for $C_{46}H_{40}Br_4N_{16}Au$ [M − Cl$^+$], m/z 1329.0021. Found, m/z 1329.0056.

The triazolyl-functionalised (NHC)Au^{III}Cl$_3$ complex 12. The triazolyl-functionalised (NHC)AuCl complex **8** (50.0 mg, 0.062 mmol) dissolved in DCM (10 mL), thionyl chloride (1.00 mL, 13.8 mmol) was added, and the mixture heated at reflux for 2 days under N_2. The solvent was removed under vacuum and the residue was washed with diethyl ether (3 × 5 mL) to leave the product as a yellow powder (53.5 mg, 97%). ^{1}H NMR (500 MHz, CD_2Cl_2): δ 7.86 (s, 2H, H8), 7.63 (2H, dd, $^3J_{H,H}$ = 7.8, $^4J_{H,H}$ = 1.2 Hz, H14), 7.42 (s, 2H, H4/H5), 7.34 (2H, apparent td, "triplet" splitting 7.5 Hz, $^4J_{H,H}$ = 1.2 Hz, H12), 7.26 (2H, apparent td, "triplet" splitting 7.8 Hz, $^4J_{H,H}$ = 1.7 Hz, H13), 7.22 (2H, dd, $^3J_{H,H}$ = 7.5 Hz, $^4J_{H,H}$ = 1.7 Hz, H11), 5.64 (s, 4H, H9), 5.51 (s, 4H, H6). ^{13}C NMR (125.7 MHz, CD_2Cl_2): δ 140.8 (C2), 140.5 (C7), 134.0 (C10), 133.6 (C14), 131.1 (C11), 131.0 (C13), 128.6 (C12), 125.1 (C8), 124.5 (C4/C5), 124.0 (C15), 54.5 (C9), 46.3 (C6). Microanalysis: found: C, 31.84; H, 2.30; N, 12.53% $C_{23}H_{20}AuBr_2Cl_3N_8$ requires C, 31.69; H, 2.31; N, 12.86%. Crystals suitable for X-ray diffraction studies were grown by diffusion of vapours between pentane and a solution of the complex in DCM.

The triazolyl-functionalised [(NHC)$_2$Au^{III}Cl$_2$]Cl complex 14. Method 1: the triazolyl-functionalised (NHC)AuCl complex **10** (9.0 mg, 6.60 μmol) was suspended in DCM (10 mL), thionyl chloride (0.12 mL, 1.64 mmol) was added, and the mixture heated at reflux for 4 days under N_2. The solvent was removed under vacuum, the residue was stirred with diethyl ether, and the diethyl ether was decanted off, to leave the product as a yellow solid (8.3 mg, 82%).

Method 2: the triazolyl-functionalised (NHC)AuCl complex **10** (15.8 mg, 11.5 μmol) was dissolved in thionyl chloride (3 mL) and the mixture heated at reflux for 5 days under N_2. The solvent was removed under vacuum, the residue was stirred with diethyl ether, and the diethyl ether decanted off, to leave the product as a yellow solid (15 mg, 86%). ^{1}H NMR (600 MHz, DMSO-d_6) NHC–Au^{III}: δ 8.21 (s, 4H, H8), 7.82 (s, 4H, H4/H5), 7.64 (4H, br d, $^3J_{H,H}$ = 7.5 Hz, H14), 7.29 (8H, m, H12 and H11), 7.08 (4H, br d, $^3J_{H,H}$ = 7.3 Hz, H13), 5.80 (s, 8H, H6), 5.64 (s, 8H, H9). ^{13}C NMR (150.9 MHz, DMSO-d_6) NHC–Au^{III}. δ 151.7 (C2), 141.3 (C7), 134.4 (C10), 132.9 (C14), 130.4 (C11), 130.4 (C13), 128.2 (C12), 124.9 (C8), 124.5 (C4/C5), 122.8 (C15), 53.0 (C6), 44.6 (C9). Microanalysis: found: C, 34.07; H, 2.85; N, 12.76% $C_{46}H_{40}AuBr_4Cl_3N_{16}$. $(CH_2Cl_2)_{3.5}$ requires C, 34.23; H, 2.73; N, 12.90%.

Attempted synthesis of triazolyl-functionalised Au^{III}–NHC complexes directly from KAuCl$_4$ (formation of 8, 12, 14). A mixture of Ag_2O (10.4 mg, 0.045 mmol) and the bis(triazolyl) imidazolium salt **6** (50 mg. 0.081 mmol) in DCM (10 mL) was stirred at room temperature in the absence of light overnight. $KAuCl_4$ (30.0 mg, 0.081 mmol) was added and the mixture was stirred for 10 days. The mixture was filtered through Celite. The filtrate was evaporated under vacuum and the residue was crystallised from DCM/diethyl ether to afford a yellow powder (42 mg). The ^{1}H NMR spectrum of a sample of the powder in DMSO-d_6 showed signals due **8**, **12**, **14** in a ratio of 6 : 31 : 25 respectively.

The chelate Au^{III} complex 15

(i) Synthesis using three equivalents of AgNO$_3$. A solution of $AgNO_3$ (3.20 mg, 18.7 μmol) in DMSO-d_6 (0.25 mL) was added to a solution of the Au^{III} complex **12** (5.00 mg, 5.70 μmol) in DMSO-d_6 (0.25 mL) in an NMR tube. A white precipitate (presumed to be AgCl) formed immediately. The compound remaining in solution was identified as by its ^{1}H and ^{13}C NMR spectrum.

(ii) Synthesis using two equivalents of AgNO$_3$. A solution of $AgNO_3$ (3.40 mg, 19.98 μmol) in DMSO-d_6 (0.25 mL) was added to a solution of the Au^{III} complex **12** (8.00 mg, 9.18 μmol) in DMSO-d_6 (0.25 mL) in an NMR tube. A white precipitate (presumed to be AgCl) formed immediately and the presence of Au^{III} complex **15** in solution was confirmed by ^{1}H NMR spectroscopy. The clear solution was separated from the precipitate using a pipette and the solvent was evaporated under a flow of N_2. The solid was swirled with DCM (3 mL), the DCM was drawn off by pipette and the process was repeated. The white powder that remained was dried under vacuum. Yield: 4.8 mg, 56%. ^{1}H NMR (500 MHz, DMSO-d_6): δ 9.03 (s, 2H, H8), 7.99 (s, 2H, H4/H5), 7.75 (2H, dd, $^3J_{H,H}$ = 8.0 Hz, $^4J_{H,H}$ = 1.0 Hz, H14), 7.54–7.49 (4H, m, H11 and H12), 7.40 (2H, ddd, $^3J_{H,H}$ = 8.0 Hz $^3J_{H,H}$ = 7.1 Hz, $^4J_{H,H}$ = 2.1 Hz, H13), 6.08 (s, 4H, H9), 5.82 (s, 4H, H6). ^{13}C NMR (125.7 MHz, DMSO-d_6): δ 137.9 (C2), 133.2 (C14), 132.2 (C7), 132.0 (C10), 131.9 (C11), 131.6 (C13), 128.5 (C12), 128.1 (C8), 123.8 (C15), 123.7 (C4/C5), 56.5 (C9), 44.5 (C6).

Microanalysis: found: C, 28.09; H, 2.21; N, 13.98%. $C_{23}H_{20}AuBr_2ClN_{10}O_6$. $(CH_2Cl_2)_{1.2}$ requires C, 28.31; H, 2.20; N, 13.64%.

Data availability

The data supporting this article have been included as part of the ESI.† More raw data are available from the corresponding author on reasonable request.

Author contributions

Hawraa S. Al-Buthabhak: synthesis and characterisation, formal analysis; investigation; methodology; writing – original draft. Karrar Al-Ameed: computational calculations; formal analysis; investigation Yu Yu: methodology. Alexandre Sobolev: data curation; formal analysis; investigation. Stephen Moggach: data curation; formal analysis; investigation. Hani Al-Salami: resources. Vito Ferro: supervision; writing – review and editing. Murray V. Baker: supervision; resources; writing – review and editing.

Conflicts of interest

There are no conflicts of interest to declare.

Acknowledgements

The authors acknowledge the facilities and the scientific and technical assistance of the Australian Microscopy & Microanalysis Research Facility at the Centre for Microscopy, Characterisation & Analysis, the University of Western Australia. Hawraa S. Al-Buthabhak thanks the Higher Committee for Education Development in Iraq (HCED) for financial support. Al-Salami is supported by the European Union Horizon 2020 Research Project and Innovation Program under the Marie Skłodowska-Curie Grant Agreement No. 872370, Curtin Faculty ORS-WAHAI Consortium, and the Australian National Health and Medical Research Council (NHMRC, APP9000597). Stephen A. Moggach thanks the Australian Research Council (ARC) for a Future Fellowship (FT200100243). We thank the University of Western Australia and the University of Queensland for a UWA-UQ Partnership Research Collaboration Award (to VF and MVB).

References

1 W. Zhao, V. Ferro and V. M. Baker, *Coord. Chem. Rev.*, 2017, **339**, 1–16.
2 M. N. Hopkinson, C. Richter, M. Schedler and F. Glorius, *Nature*, 2014, **510**, 485–496.
3 P. Mathew, A. Neels and M. Albrecht, *J. Am. Chem. Soc.*, 2008, **130**, 13534–13535.
4 R. Jothibasu and H. V. Huynh, *Chem. Commun.*, 2010, **46**, 2986–2988.
5 J. Turek, I. Panov, P. Svec, Z. Ruzickova and A. Ruzicka, *Dalton Trans.*, 2014, **43**, 15465–15474.
6 M. V. Baker, P. J. Barnard, S. J. Berners-Price, S. K. Brayshaw, J. L. Hickey, B. W. Skelton and A. H. White, *Dalton Trans.*, 2006, 3708–3714, DOI: **10.1039/b602560a**.
7 N. Hamdi, I. Slimani, L. Mansour, F. Alresheedi, N. Gürbüz and I. Özdemir, *New J. Chem.*, 2021, **45**, 21248–21262.
8 A. Martínez, J. L. Krinsky, I. Peñafiel, S. Castillón, K. Loponov, A. Lapkin, C. Godard and C. Claver, *Catal. Sci. Technol.*, 2015, **5**, 310–319.
9 B. Jacques, D. Hueber, S. Hameury, P. Braunstein, P. Pale, A. Blanc and P. de Frémont, *Organometallics*, 2014, **33**, 2326–2335.
10 M. Bouhrara, E. Jeanneau, L. Veyre, C. Coperet and C. Thieuleux, *Dalton Trans.*, 2011, **40**, 2995–2999.
11 A. S. Hashmi, T. Lauterbach, P. Nösel, M. H. Vilhelmsen, M. Rudolph and F. Rominger, *Chem.–Eur. J.*, 2013, **19**, 1058–1065.
12 A. S. K. Hashmi, A. M. Schuster and F. Rominger, *Angew. Chem., Int. Ed.*, 2009, **48**, 8247–8249.
13 A. G. Nair, R. T. McBurney, M. R. D. Gatus, S. C. Binding and B. A. Messerle, *Inorg. Chem.*, 2017, **56**, 12067–12075.
14 C. Hemmert and H. Gornitzka, *Dalton Trans.*, 2016, **45**, 440–447.
15 P. J. Barnard, L. E. Wedlock, M. V. Baker, S. J. Berners-Price, D. A. Joyce, B. W. Skelton and J. H. Steer, *Angew. Chem., Int. Ed.*, 2006, **45**, 5966–5970.
16 Ö. Karaca, S. M. Meier-Menches, A. Casini and F. E. Kühn, *Chem. Commun.*, 2017, **53**, 8249–8260.
17 T. Zou, C. T. Lum, S. S. Chui and C. M. Che, *Angew. Chem., Int. Ed.*, 2013, **52**, 2930–2933.
18 G. Gasser, I. Ott and N. Metzler-Nolte, *J. Med. Chem.*, 2011, **54**, 3–25.
19 L. E. Wedlock and S. J. Berners-Price, *Aust. J. Chem.*, 2011, **64**, 692–704.
20 J. J. Soldevila-Barreda and N. Metzler-Nolte, *Chem. Rev.*, 2019, **119**, 829–869.
21 S. Y. Hussaini, R. A. Haque and M. R. Razali, *J. Organomet. Chem.*, 2019, **882**, 96–111.
22 H. S. Al-Buthabhak, Y. Yu, A. Sobolev, H. Al-Salami and M. V. Baker, *J. Inclusion Phenom. Macrocyclic Chem.*, 2021, **101**, 227–242.
23 T. Zou, C. N. Lok, P. K. Wan, Z. F. Zhang, S. K. Fung and C. M. Che, *Curr. Opin. Chem. Biol.*, 2018, **43**, 30–36.
24 J. L. Hickey, R. A. Ruhayel, P. J. Barnard, M. V. Baker, S. J. Berners-Price and A. Filipovska, *J. Am. Chem. Soc.*, 2008, **130**, 12570–12571.
25 G. Achar, S. A. Patil, J. G. Małecki and S. Budagumpi, *New J. Chem.*, 2019, **43**, 1216–1229.
26 S. J. Berners-Price and A. Filipovska, *Metallomics*, 2011, **3**, 863–873.
27 G. Moreno-Alcántar, P. Picchetti and A. Casini, *Angew. Chem., Int. Ed.*, 2023, **62**, e202218000.
28 B. S. Murray and P. J. Dyson, *Curr. Opin. Chem. Biol.*, 2020, **56**, 28–34.
29 G. Augello, A. Azzolina, F. Rossi, F. Prencipe, G. F. Mangiatordi, M. Saviano, L. Ronga, M. Cervello and D. Tesauro, *Pharmaceutics*, 2023, **15**, 466.

30 H. S. Al-Buthabhak, V. Falasca, Y. Yu, A. N. Sobolev, B. W. Skelton, S. A. Moggach, V. Ferro, H. Al-Salami and M. V. Baker, *Appl. Organomet. Chem.*, 2022, **38**, e6645.
31 M. G. Gardiner and C. C. Ho, *Coord. Chem. Rev.*, 2018, **375**, 373–388.
32 M. A. W. Lawrence, K.-A. Green, P. N. Nelson and S. C. Lorraine, *Polyhedron*, 2018, **143**, 11–27.
33 M. Navarro, A. Tabey, G. Szalóki, S. Mallet-Ladeira and D. Bourissou, *Organometallics*, 2021, **40**, 1571–1576.
34 B. Schulze and U. S. Schubert, *Chem. Soc. Rev.*, 2014, **43**, 2522–2571.
35 K. F. Donnelly, A. Petronilho and M. Albrecht, *Chem. Commun.*, 2013, **49**, 1145–1159.
36 M. Albrecht, *Adv. Organomet. Chem.*, 2014, **62**, 111–158.
37 M. Delgado-Rebollo, D. Canseco-Gonzalez, M. Hollering, H. Mueller-Bunz and M. Albrecht, *Dalton Trans.*, 2014, **43**, 4462–4473.
38 M. Hollering, M. Albrecht and F. E. Kühn, *Organometallics*, 2016, **35**, 2980–2986.
39 D. Canseco-Gonzalez, A. Petronilho, H. Mueller-Bunz, K. Ohmatsu, T. Ooi and M. Albrecht, *J. Am. Chem. Soc.*, 2013, **135**, 13193–13203.
40 P. Font, H. Valdés, G. Guisado-Barrios and X. Ribas, *Chem. Sci.*, 2022, **13**, 9351–9360.
41 H. Duan, S. Sengupta, J. L. Petersen, N. G. Akhmedov and X. Shi, *J. Am. Chem. Soc.*, 2009, **131**, 12100–12102.
42 D. Wang, Y. Zhang, A. Harris, L. N. S. Gautam, Y. Chen and X. Shi, *Adv. Synth. Catal.*, 2011, **353**, 2584–2588.
43 Y. Yang, W. Hu, X. Ye, D. Wang and X. Shi, *Adv. Synth. Catal.*, 2016, **358**, 2583–2588.
44 C. Lang, K. Pahnke, C. Kiefer, A. S. Goldmann, P. W. Roesky and C. Barner-Kowollik, *Polym. Chem.*, 2013, **4**, 5456–5462.
45 M. Baron, S. Bellemin-Laponnaz, C. Tubaro, M. Basato, S. Bogialli and A. Dolmella, *J. Inorg. Biochem.*, 2014, **141**, 94–102.
46 V. Lewe, M. Preuss, E. A. Woźnica, D. Spitzer, R. Otter and P. Besenius, *Chem. Commun.*, 2018, **54**, 9498–9501.
47 M. Monticelli, S. Bellemin-Laponnaz, C. Tubaro and M. Rancan, *Eur. J. Inorg. Chem.*, 2017, **2017**, 2488–2495.
48 M. Monticelli, M. Baron, C. Tubaro, S. Bellemin-Laponnaz, C. Graiff, G. Bottaro, L. Armelao and L. Orian, *ACS Omega*, 2019, **4**, 4192–4205.
49 A. Longhi, M. Baron, M. Rancan, G. Bottaro, P. Sgarbossa and C. Tubaro, *Molecules*, 2019, **24**, 2305.
50 T. Eybe, T. Bohn, J. N. Audinot, T. Udelhoven, H. M. Cauchie, H. N. Migeon and L. Hoffmann, *Chemosphere*, 2009, **76**, 134–140.
51 D. Rodríguez-Hernández, A. J. Demuner, L. C. A. Barbosa, L. Heller and R. Csuk, *Eur. J. Med. Chem.*, 2016, **115**, 257–267.
52 H. M. J. Wang and I. J. B. Lin, *Organometallics*, 1998, **17**, 972–975.
53 A. Collado, A. Gomez-Suarez, A. R. Martin, A. M. Slawin and S. P. Nolan, *Chem. Commun.*, 2013, **49**, 5541–5543.
54 M. Pažický, A. Loos, M. J. Ferreira, D. Serra, N. Vinokurov, F. Rominger, C. Jäkel, A. S. K. Hashmi and M. Limbach, *Organometallics*, 2010, **29**, 4448–4458.
55 S. Zhu, R. Liang, L. Chen, C. Wang, Y. Ren and H. Jiang, *Tetrahedron Lett.*, 2012, **53**, 815–818.
56 P. de Fremont, R. Singh, E. D. Stevens, J. L. Petersen and S. P. Nolan, *Organometallics*, 2007, **26**, 1376–1385.
57 A. H. Mageed, B. W. Skelton and M. V. Baker, *Dalton Trans.*, 2017, **46**, 7844–7856.
58 C. Hirtenlehner, C. Krims, J. Holbling, M. List, M. Zabel, M. Fleck, R. J. Berger, W. Schoefberger and U. Monkowius, *Dalton Trans.*, 2011, **40**, 9899–9910.
59 S. Ahmad, A. A. Isab, H. P. Perzanowski, M. S. Hussain and N. M. Akhtar, *Transit. Met. Chem.*, 2002, **27**, 177–183.
60 S. Zhu, R. Liang and H. Jiang, *Tetrahedron*, 2012, **68**, 7949–7955.
61 H. Ibrahim, P. de Frémont, P. Braunstein, V. Théry, L. Nauton, F. Cisnetti and A. Gautier, *Adv. Synth. Catal.*, 2015, **357**, 3893–3900.
62 R. Jothibasu, H. V. Huynh and L. L. Koh, *J. Organomet. Chem.*, 2008, **693**, 374–380.
63 H. V. Huynh, S. Guo and W. Wu, *Organometallics*, 2013, **32**, 4591–4600.
64 M. V. Baker, P. J. Barnard, S. J. Berners-Price, S. K. Brayshaw, J. L. Hickey, B. W. Skelton and A. H. White, *J. Organomet. Chem.*, 2005, **690**, 5625–5635.
65 W. A. Herrmann, O. Runte and G. Artus, *J. Organomet. Chem.*, 1995, **501**, C1–C4.
66 Y.-P. Huang, C.-C. Tsai, W.-C. Shih, Y.-C. Chang, S.-T. Lin, G. P. A. Yap, I. Chao and T.-G. Ong, *Organometallics*, 2009, **28**, 4316–4323.
67 H. V. Huynh, C. H. Yeo and Y. X. Chew, *Organometallics*, 2010, **29**, 1479–1486.
68 H. Günther, *NMR Spectroscopy, Basic Principles, Concepts, and Applications in Chemistry*, Wiley, 2nd edn, 1995, vol. 343.
69 K. D. Zimmer, R. Shoemaker and R. R. Ruminski, *Inorg. Chim. Acta*, 2006, **359**, 1478–1484.
70 H. V. Huynh and J. Wu, *J. Organomet. Chem.*, 2009, **694**, 323–331.
71 P. W. Atkins and J. de Paula, *Physical Chemistry*, Oxford University Press, 2010.
72 M. Hricovíni, J. Asher and M. Hricovíni, *RSC Adv.*, 2020, **10**, 5540–5550.
73 J. Kujawski, K. Czaja, T. Ratajczak, E. Jodłowska and M. K. Chmielewski, *Molecules*, 2015, **20**(7), 11875–11190.
74 M. Boronat, A. Corma, C. González-Arellano, M. Iglesias and F. Sánchez, *Organometallics*, 2010, **29**, 134–141.
75 A. Bondi, *J. Phys. Chem.*, 1964, **68**, 441–451.
76 S. Alvarez, *Dalton Trans.*, 2013, **42**, 8617–8636.
77 D. Piovesan, G. Minervini and S. C. Tosatto, *Nucleic Acids Res.*, 2016, **44**, W367–W374.
78 P. de Fremont, N. M. Scott, E. D. Stevens and S. P. Nolan, *Organometallics*, 2005, **24**, 2411–2418.
79 M. V. Baker, P. J. Barnard, S. K. Brayshaw, J. L. Hickey, B. W. Skelton and A. H. White, *Dalton Trans.*, 2005, 37–43, DOI: **10.1039/b412540a**.
80 H. M. J. Wang, C. Y. L. Chen and I. J. B. Lin, *Organometallics*, 1999, **18**, 1216–1223.
81 H. Sivaram, J. Tan and H. V. Huynh, *Organometallics*, 2012, **31**, 5875–5883.

82 B. Jacques, J. Kirsch, P. de Frémont and P. Braunstein, *Organometallics*, 2012, **31**, 4654–4657.
83 S. Gaillard, A. M. Z. Slawin, A. T. Bonura, E. D. Stevens and S. P. Nolan, *Organometallics*, 2010, **29**, 394–402.
84 M. Baron, C. Tubaro, M. Basato, A. Biffis, M. M. Natile and C. Graiff, *Organometallics*, 2011, **30**, 4607–4615.
85 H. V. Huynh, Y. Han, J. H. H. Ho and G. K. Tan, *Organometallics*, 2006, **25**, 3267.
86 M. Porchia, M. Pellei, M. Marinelli, F. Tisato, F. Del Bello and C. Santini, *Eur. J. Med. Chem.*, 2018, **146**, 709–746.
87 T. Zou, C. T. Lum, C. N. Lok, J. J. Zhang and C. M. Che, *Chem. Soc. Rev.*, 2015, **44**, 8786–8801.
88 C. Marzano, V. Gandin, A. Folda, G. Scutari, A. Bindoli and M. P. Rigobello, *Free Radic. Biol. Med.*, 2007, **42**, 872–881.
89 J. H. Kim, E. Reeder, S. Parkin and S. G. Awuah, *Sci. Rep.*, 2019, **9**, 12335.
90 P. C. Kunz, M. U. Kassack, A. Hamacher and B. Spingler, *Dalton Trans.*, 2009, **37**, 7741–7747.
91 X. Zhou and L. Zhou, *Theor. Chem. Acc.*, 2016, **135**, 30.
92 M.-C. Brandys, M. C. Jennings and R. J. Puddephatt, *J. Chem. Soc., Dalton Trans.*, 2000, **24**, 4601–4606.
93 A. D. Becke, *J. Chem. Phys.*, 1993, **98**, 5648–5652.
94 C. Lee, W. Yang and R. G. Parr, *Phys. Rev. B: Condens. Matter Mater. Phys.*, 1988, **37**, 785.
95 F. Weigend and R. Ahlrichs, *Phys. Chem. Chem. Phys.*, 2005, **7**, 3297–3305.
96 M. J. Frisch, G. W. Trucks, H. B. Schlegel, G. E. Scuseria, M. A. Robb, J. R. Cheeseman, G. Scalmani, V. Barone, G. A. Petersson, H. Nakatsuji, X. Li, M. Caricato, A. V. Marenich, J. Bloino, B. G. Janesko, R. Gomperts, B. Mennucci, H. P. Hratchian, J. V. Ortiz, A. F. Izmaylov, J. L. Sonnenberg, D. Williams-Young, F. Ding, F. Lipparini, F. Egidi, J. Goings, B. Peng, A. Petrone, T. Henderson, D. Ranasinghe, V. G. Zakrzewski, J. Gao, N. Rega, G. Zheng, W. Liang, M. Hada, M. Ehara, K. Toyota, R. Fukuda, J. Hasegawa, M. Ishida, T. Nakajima, Y. Honda, O. Kitao, H. Nakai, T. Vreven, K. Throssell, J. A. Montgomery Jr, J. E. Peralta, F. Ogliaro, M. J. Bearpark, J. J. Heyd, E. N. Brothers, K. N. Kudin, V. N. Staroverov, T. A. Keith, R. Kobayashi, J. Normand, K. Raghavachari, A. P. Rendell, J. C. Burant, S. S. Iyengar, J. Tomasi, M. Cossi, J. M. Millam, M. Klene, C. Adamo, R. Cammi, J. W. Ochterski, R. L. Martin, K. Morokuma, O. Farkas, J. B. Foresman and D. J. Fox, *Gaussian 16, Revision C.01*, Wallingford, CT, 2016.
97 H. Schröder, A. Creon and T. Schwabe, *J. Chem. Theory Comput.*, 2015, **11**, 3163–3170.
98 G. M. Sheldrick, *Acta Crystallogr., Sect. C: Cryst. Struct. Commun.*, 2015, **71**, 3–8.
99 T. Mosmann and J. lmmun, *Methods*, 1983, **65**, 55–63.